Estimating temporal variation in transmission of SARS-CoV-2 and physical distancing behaviour in Australia

Technical Report 17 July 2020

Nick Golding[1], Freya M. Shearer[2], Robert Moss[2], Peter Dawson[3], Dennis Liu[4], Joshua V. Ross[4], Rob Hyndman[5], Cameron Zachreson[6], Nic Geard[2,6,7], Jodie McVernon[2,7,8], David J. Price[2,7], and James M. McCaw[2,7,9]

1. Telethon Kids Institute and Curtin University, Perth, Australia
2. Melbourne School of Population and Global Health, The University of Melbourne, Australia
3. Defence Science and Technology, Department of Defence, Australia
4. School of Mathematical Sciences, The University of Adelaide, Australia
5. Department of Econometrics and Business Statistics, Monash University, Australia
6. School of Computing and Information Systems, The University of Melbourne, Australia
7. Peter Doherty Institute for Infection and Immunity, The Royal Melbourne Hospital and The University of Melbourne, Australia
8. Murdoch Children's Research Institute, The Royal Children's Hospital, Australia
9. School of Mathematics and Statistics, The University of Melbourne, Australia

Key messages

The focus of this report is on the period from early June up to 1 July 2020. As of 17 July (the time of public release of this report), we acknowledge that the outbreak in metropolitan Melbourne (Victoria) is ongoing, and that there are early signs of increasing epidemic activity in New South Wales, which we are currently investigating and will be the subject of future reports.

Estimates of changes in physical distancing behaviour

- We use data from nationwide surveys and mobility data from technology companies to estimate trends in macro-distancing and micro-distancing behaviour over time.
- As of 1 July, this analysis suggests that levels of both macro-distancing and micro-distancing behaviour have waned since peak adherence in early April. See Figures 1–3 and Table 1.
- Encouragingly, there is evidence of decreased levels of population mobility in Victorian LGAs over the last week of June, most markedly in LGAs containing postcodes where "Stay at Home" restrictions have been active in response to the current outbreak (Figure 4).

Estimates of current epidemic activity

- We report estimates of local transmission potential from a statistical method which allows us to distinguish between transmission in the general population and clusters/localised outbreaks (Figure 5).
- As of 1 July, average state-wide transmission potential is estimated to be above 1 in all states/territories, except Victoria (See Figure 6 and Table 2).
- In Victoria, the one state with a substantial number of active cases, there is strong evidence for substantial deviation from state-level transmission potential, consistent with a

substantial cluster or a number of smaller clusters (Figure 7). This has resulted in an estimated R_{eff} of 1.3 [1.04, 1.7] for active cases in Victoria (97% chance of exceeding R_{eff} =1), indicative of an active, growing outbreak. However, if this activity can be brought under control, the state-wide transmission potential of 0.92 [0.81–1.1], suggests that there is perhaps sufficient maintenance of distancing behaviours to avoid further escalation of epidemic activity.

- An analysis of the temporal trend of R_{eff} in Victoria since the beginning of the outbreak (late June) reveals that following an initial sharp rise in R_{eff} from below to well above 1, the R_{eff} has steadily decreased over the past two weeks. At all times, the R_{eff} has been above 1, indicative of a growing outbreak. The declining R_{eff} suggests that control is possible with continued enactment of response measures and community compliance.

Forecasts of the daily number of new local cases

- We report state-level forecasts of the daily number of new local cases up to 3 August, *synthesised* from three independent models (known as an 'ensemble forecast').
- If local transmission potential remains at its current estimated level (as of 1 July), we anticipate that daily local case counts will remain very low or zero into August for all states/territories except Victoria (Figure 9).
- Forecasts for Victoria are highly uncertain at this time. A substantial increasing caseload into August is possible. A decrease is also plausible (Figures 10 and 11).

Forecasting alternate scenarios of the June outbreak in Victoria

- A scenario analysis was performed to assess the potential impact of alternate scenarios on the Victorian outbreak.
- Estimates of the R_{eff} of local active cases for Victoria as of 1 July were projected forward from 4 July through to 3 August for three alternate scenarios:
  - Scenario 0: The forecast based on current estimates of local transmission potential
  - Scenario 1: State-wide distancing behaviour returned to levels estimated on 13 May
  - Scenario 2: State-wide distancing behaviour returned to peak levels of adherence (which is estimated to have occurred in Victoria on 13 April)
  - Scenario 3: Overall public health response at peak level of impact (Component 2 of R_{eff} from 29 March and Component 1 of R_{eff} from 13 April)
- If peak levels of transmission mitigation (Scenario 3) were achieved, this would result in a rapid decline in cases over the coming month (Figure 15). However, more likely is an intermediate effect (Scenario 1 or 2) in which control is achieved but with slowly declining epidemic activity over the next month (Figures 13 and 14). Note: even with improved transmission mitigation, epidemic growth is possible (upper credible intervals in Figures 13 and 14).

Estimating trends in distancing behaviour

Overview

To investigate the impact of distancing measures on SARS-CoV-2 transmission, we distinguish between two types of distancing behaviour: 1) macro-distancing *i.e.*, reduction in the rate of non-household contacts; and 2) micro-distancing *i.e.*, reduction in transmission probability per non-household contact.

We used data from nationwide surveys to estimate trends in specific macro-distancing (average daily number of non-household contacts) and micro-distancing (proportion of the population always keeping 1.5m physical distance from non-household contacts) behaviours over time. We used these survey data to infer state-level trends in macro- and micro-distancing behaviour over time, with additional information drawn from trends in mobility data.

Results

This analysis suggests that levels of both macro-distancing and micro-distancing behaviour peaked around 8–12 April, and both behaviours have subsequently waned:

- **The average daily number of non-household contacts (macro-distancing) reached its minimum around 12 April and ranged from 2.7–5.7. This is estimated to have waned to 5.9–11.5 by 1 July**. See Figure 1 and Table 1.
- **Peak adherence to the 1.5m rule (micro-distancing) occurred around 8 April and ranged from 60.2%–63.1% across the states/territories. This is estimated to have waned to 27.9%–39.1% by 1 July**. See Figure 2 and Table 1.

Increased population mobility and non-household contact rates (macro-distancing) are expected given the easing of restrictions since early May. However, keeping 1.5m away from others (micro-distancing) has remained the public health advice over this period.

Table 1: Left columns: estimates of the average daily number of non-household contacts (macro-distancing) at peak adherence on around 12 April and as of 1 July for each state/territory. Right columns: estimates of self-reported adherence to the 1.5m rule (micro-distancing) at peak adherence on around 8 April and as of 1 July for each state/territory.

	Non-household contacts		Adherence to 1.5m rule	
State	Peak [90% CrI]	1 July [90% CrI]	Peak [90% CrI]	1 July [90% CrI]
ACT	2.9 [2.7,3.2]	7.5 [7.2,7.9]	61.9% [58.8,64.4]	32.3% [28.0,36.2]
NSW	3.2 [3.1,3.5]	8.1 [7.6,8.6]	63.1% [61.4,64.9]	35.9% [33.7,38.1]
NT	5.7 [5.2,6.2]	11.5 [10.7,12.3]	60.2% [54.5,63.6]	27.9% [20.9,33.9]
Qld	4.3 [4.1,4.5]	8.6 [8.3,9]	62.4% [60.4,64.3]	39.1% [36.5,41.6]
SA	4.2 [3.8,4.6]	8.2 [7.7,8.5]	61.2% [58.6,63.5]	33.5% [31.0,35.9]
Tas	3.4 [2.9,4.0]	7.5 [6.9,7.8]	62.6% [59.9,65.2]	37.1% [33.3,41.3]
Vic	2.7 [2.5,2.9]	5.9 [5.7,6.1]	62.8% [61.1,64.6]	35.9% [33.7,38.1]
WA	4.3 [4.0,4.6]	9.4 [8.8,10.0]	61.5% [59.0,63.7]	31.2% [28.7,33.6]

These state-level macro- and micro-distancing trends were then used in the model of R_{eff} to inform the reduction in non-household transmission rates (Figures S5 and S6).

Population mobility analysis

Overview

A number of data streams provide information on mobility before and in response to COVID-19 across Australian states/territories. Each of these data streams represents a different aspect of population mobility, but they show some common trends — reflecting underlying changes in behaviour. We use a latent variable statistical model to simultaneously analyse these data streams and quantify the underlying behavioural variables. Full details of this analysis is provided in our Technical Report dated 15 May 2020 (`https://www.doherty.edu.au/about/reports-publications`).

Results

The model detects a decline in the physical distancing variable over time (*i.e.*, increasing mixing) since the date of peak adherence to these measures, $\approx$ 2 April (see Figure 3). **Specifically, by 1 July, the impact of physical distancing on time at parks is expected to have reduced by 69% on average across states (ranging from 26% in Tas to 100% in ACT, NT, and Qld), the effect on requests for driving directions by 90% (49% in Tas to 100% in ACT, NSW, NT, Qld, and WA), and the effect on time at transit stations by 37% (25% in Vic to 44% in NSW).**

The largest reductions in the impacts of physical distancing are evident in mobility data streams for lower transmission risk activities, such as time at parks. There is also a clear reduction in data streams representing higher-risk activities, such as time at workplaces. However, these mobility data do not indicate whether the increase in higher transmission risk activities is mitigated by other behaviours that are not measured by these metrics — such as reducing contacts and adherence to the $4m^2$ rule. In other words, while changes in these mobility data streams are useful for detecting changes in macro-distancing behaviour, they do not capture changes in micro-distancing behaviour.

Plots of each data stream and our model fits for each state and territory are shown in the Appendix (Figures S8–S14)

Figure 1: Estimated trends in macro-distancing behaviour, *i.e.*, reduction in the daily rate of non-household contacts, in each state/territory (dark purple ribbons = 50% credible intervals; light purple ribbons = 90% credible intervals). Estimates are informed by state-level data from two surveys conducted by the national modelling group in early April and early May, and five BETA surveys conducted weekly from late May to late June (indicated by the black lines and grey rectangles), and an assumed pre-COVID-19 daily rate of 10.7 non-household contacts taken from previous studies. The width of the grey boxes corresponds to the duration of each survey wave (around 4 days) and the green ticks indicate the dates that public holidays coincided with survey waves (when people tend to stay home, biasing down the number of non-household contacts reported on those days). Note that the apparent increase in contacts in the second survey in Tas and WA is a statistical artefact due to the small sample sizes (100 in WA, 21 in Tas) which happen to contain two respondents reporting 100+ contacts. In general, estimates depicted by the grey rectangles are very sensitive to individuals with high numbers of contacts.

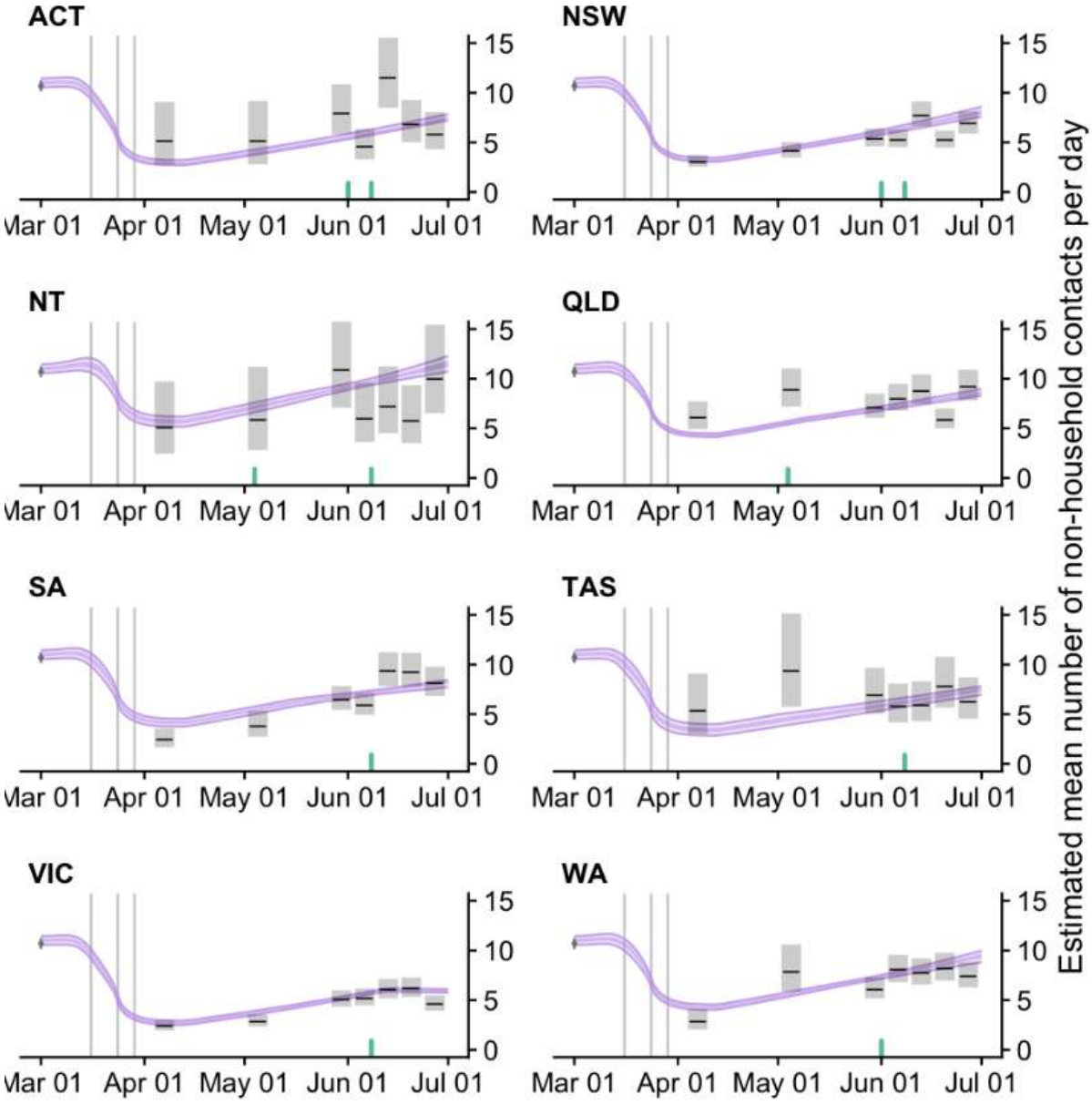

Figure 2: Estimated trends in micro-distancing behaviour, *i.e.* reduction in transmission probability per non-household contact, in each state/territory (dark purple ribbons = 50% credible intervals; light purple ribbons = 90% credible intervals). Estimates are informed by state-level data from 14 nationwide surveys conducted weekly by BETA from late March to late June (indicated by the black lines and grey boxes). The width of the grey boxes corresponds to the duration of each survey wave (around 4 days).

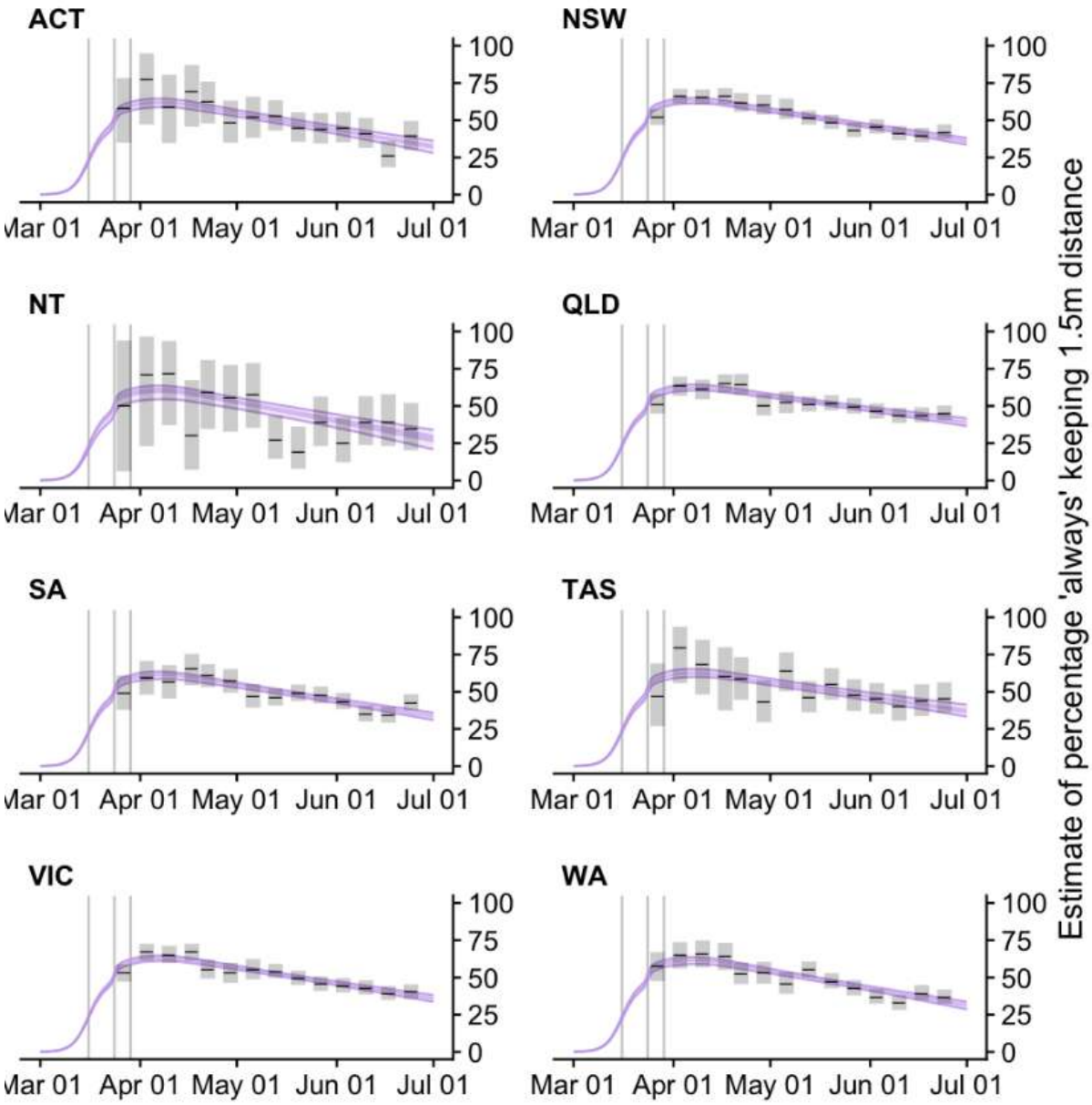

Figure 3: Percentage change compared to a pre-COVID-19 baseline of three key mobility data streams in each Australian state and territory up to 1 July. Solid vertical lines give the dates of three physical distancing measures: restriction of gatherings to 500 people or fewer; closure of bars, restaurants, and cafes; restriction of gatherings to 2 people or fewer. The dashed vertical line marks 1 July, the most recent date for which some mobility data are available. Purple dots in each panel are data stream values (percentage change on baseline). Solid lines and grey shaded regions are the posterior mean and 95% credible interval estimated by our model of the latent behaviours driving each data stream. Plots of each data stream and our model fits for each state and territory are shown in the Appendix (Figures S8–S14).

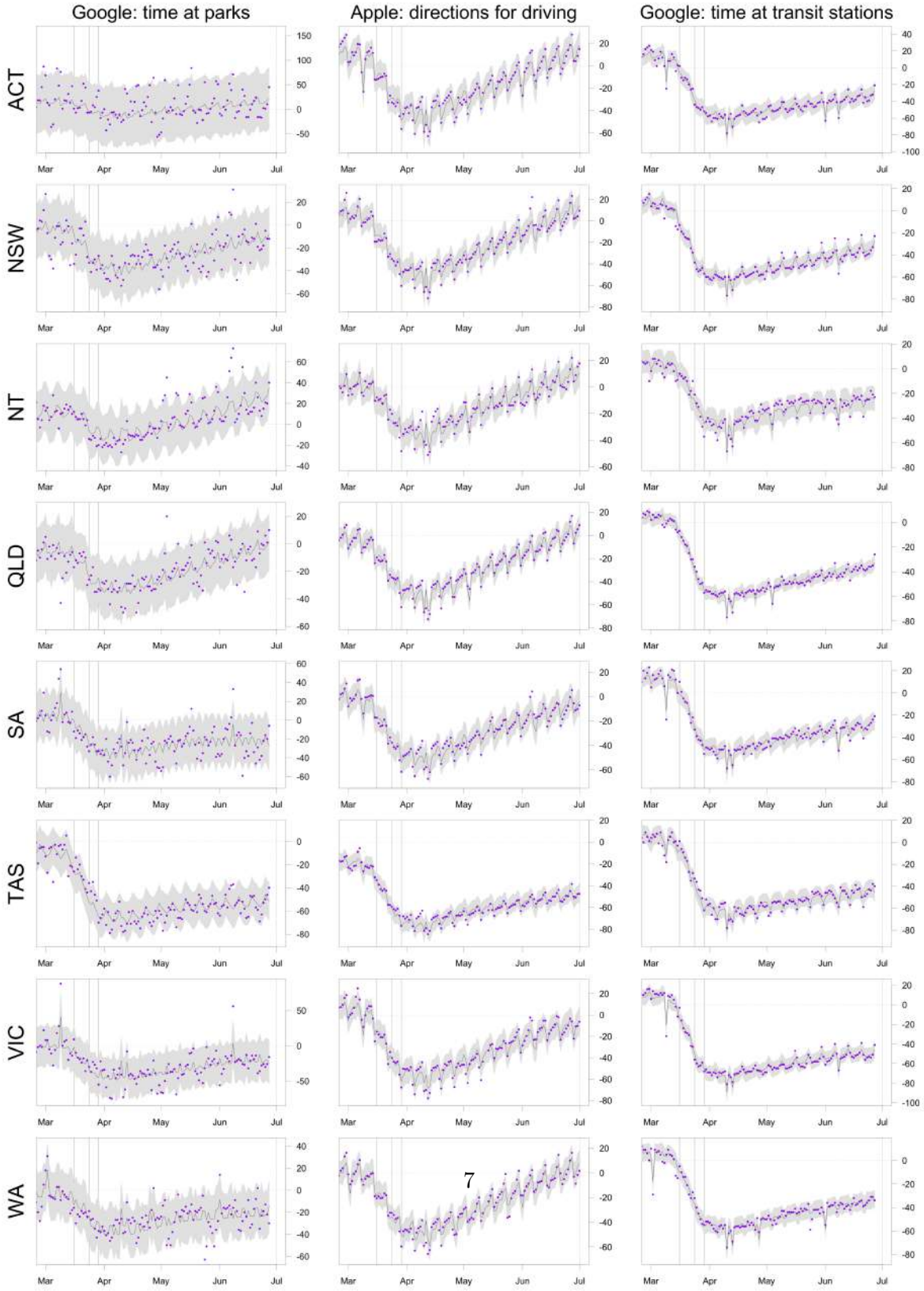

LGA-level population mobility analysis for Victoria

Overview

Facebook provide access to several aggregated and anonymised data sets on mobility for humanitarian use via their Data for Good program (`https://dataforgood.fb.com`). To preserve privacy, data are aggregated to the level of map tiles (which range in size from 0.6 km^2 to 4 km^2) or administrative regions (corresponding to Local Government Areas), and data are not provided for any tiles or regions containing a small number of users (10 to 300, depending on the data set). Here we use a movement range data set which records the proportion of Facebook users who "stay put" over the course of a day (24 hour period) aggregated by LGA.

Results

We report the proportion of users who "stayed put" each day between Saturday 29 February 2020 and Sunday 4 July 2020 (the latest date at which data are available) for each LGA in Victoria (Figure 4).

The proportion of people "staying put" increased dramatically over March, reaching a peak around Easter, and levelled off over April. From the beginning of May, this proportion steadily decreased into June. Over the past one to two weeks (*i.e.*, since late June), the proportion of people staying put in Greater Melbourne LGAs has increased compared to the preceding three weeks, most markedly in LGAs containing postcodes where "Stay at Home" advice has been in place in response to the June outbreak.

Figure 4: Proportion of Facebook users who "stayed put" each day between Saturday 29 February 2020 and Sunday 4 July 2020 (the latest date at which data are available). Each line represents a single Victorian LGA. Red lines are Brimbank, Hume, Moreland and Maribyrnong (*i.e.*, LGAs containing postcodes where "Stay at Home" advice has been in place in response to the June outbreak). Grey lines are all other Greater Melbourne LGAs. Grey vertical bars indicate weekend and Victorian public holidays. Red and green dotted vertical lines indicate the timing of government announcements increasing or decreasing (respectively) restrictions on movement and gatherings.

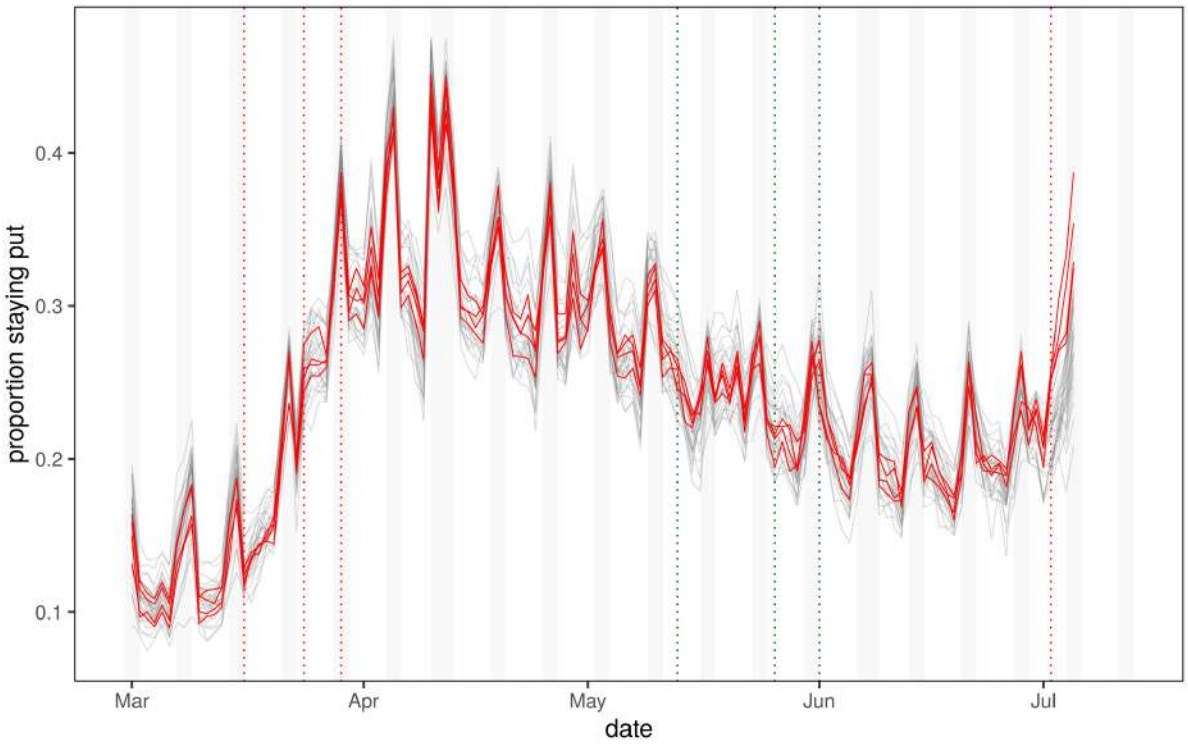

Estimating local transmission potential

We separately model local to local transmission (Figure 8) and import to local transmission for each state/territory using two components:

1. the **average state-level trend** in R_{eff} driven by population-wide interventions (specifically changes in macro- and micro-distancing behaviour, surveillance measures, and quarantine of overseas arrivals);

2. **short-term fluctuations** in R_{eff} in each state/territory to capture stochastic dynamics of transmission, such as clusters of cases and short periods of low transmission.

We have previously reported on a version of this model with three model components (Technical Report dated 15 May 2020, available from: `https://www.doherty.edu.au/about/reports-publications`) where Component 1 represented *national* trends in local transmission due to distancing behaviour. With state-level macro- and micro-distancing survey data now available, we have simplified the model structure. The model now consists of two components: state-level effects of distancing behaviour, and temporal variation representing clusters of cases.

Component 1 now reflects the average local transmission potential at state level (Figure 6), and Component 2 (previously Component 3) captures transmission within the sub-populations that have the most active cases at a given point in time (Figure 5). Component 2 is therefore useful for estimating the specific (heightened) transmission among clusters of cases in high-transmission environments — such as in healthcare workers in Tasmania and in meat processing workers in Victoria — but does not reflect changes in state-wide transmission potential (Figure 7).

Note that Component 1 for local to local transmission now also incorporates the impact of improvements in surveillance on transmission rates. Using data on the number of days from symptom onset to testing for cases, we estimate the proportion of cases that are tested (and therefore advised to isolate) by each day post-infection. We quantify how these times-to-detection have changed over time, and therefore how earlier isolation of cases due to improvements in contact tracing and clinical screening has reduced statewide R_{eff} for local to local transmission (Figure S4).

Interpretation

Where there is epidemic activity, local transmission potential of active cases (Component 1&2) is to be interpreted as the effective reproduction number, R_{eff}. In the absence of epidemic activity, Component 1&2 represents the expected amount of onward transmission from any given member of the population if they were to become infectious. In contrast, Component 1 represents the average of this over the state population, indicating the potential for the virus, if it were present, to establish and maintain community transmission (> 1) or otherwise (< 1).

Note that Component 1&2 can be higher or lower than the estimate of Component 1. In the increasing phase of a localised outbreak, it will be higher than Component 1. In the decreasing phase of a localised outbreak, Component 1&2 will be lower than Component 1 due to public health interventions, local depletion of susceptibles and/or other transmission factors that decrease the number of offspring from active cases associated with the cluster compared to that from other cases in the community.

Results

As of 1 July, in all Australia states/territories other than Victoria, average state-wide local transmission potential (Component 1) is estimated to be above 1 (Figure 6 and Table 2). For

those states/territories, this indicates that there is potential for the virus to establish itself in the population and lead to sustained community transmission.

In Victoria, the one state with a substantial number of active cases, there is strong evidence for substantial deviation from state-level transmission potential, consistent with a substantial cluster or a number of smaller clusters (Figure 7). This has resulted in an estimated R_{eff} of 1.3 [1.04, 1.7] for active cases in Victoria (97% chance of exceeding R_{eff} =1), indicative of an active, growing outbreak. However, if this activity can be brought under control, the state-wide transmission potential of 0.92 [0.81–1.1], suggests that there is perhaps sufficient maintenance of distancing behaviours to avoid further escalation of epidemic activity.

An analysis of the temporal trend of R_{eff} in Victoria since the beginning of the outbreak reveals that following an initial sharp rise in R_{eff} from below to well above 1, the R_{eff} has steadily decreased over the past two weeks. At all times, the R_{eff} has been above 1, indicative of a growing outbreak. The declining R_{eff} suggests that control is possible with continued enactment of response measures and community compliance.

Note that by the time of public release of this report, we estimate an R_{eff} of 1.39 [1.10, 1.85] for active cases in Victoria as of 13 July (99% chance of exceeding $R_{\text{eff}} = 1$). In New South Wales, we now estimate that there is an active, growing outbreak. This has resulted in an estimated R_{eff} of 1.28 [0.89, 1.82] for active cases in New South Wales as of 13 July (88% chance of exceeding R_{eff} =1).

Table 2: Estimates of local transmission potential [90% credible intervals] resulting from Component 1 (state-wide) and Component 1&2 (current active cases only) by state/territory. The total number of observed local cases with a symptom onset date recorded (or inferred) to be recorded from 22 June–6 July inclusive (*i.e.*, past 14 days) is also shown, indicative of the number of local active cases.

	Local-to-local transmission potential				
	State-wide		Current active cases only		Local cases
State	R_{eff} [90% CrI]	$P(R_{\text{eff}} > 1)$	R_{eff} [90% CrI]	$P(R_{\text{eff}} > 1)$	22 June–6 July
ACT	1.08 [0.94, 1.3]	0.85	1.1 [0.59, 2.0]	0.64	0
NSW	1.09 [0.94, 1.3]	0.84	1.0 [0.55, 1.6]	0.49	1
NT	1.51 [1.27, 1.8]	1.00	1.5 [0.78, 2.9]	0.90	1
QLD	1.06 [0.90, 1.2]	0.72	1.0 [0.46, 2.0]	0.52	1
SA	1.14 [0.99, 1.3]	0.94	1.1 [0.64, 2.0]	0.69	0
TAS	1.00 [0.85, 1.2]	0.51	1.0 [0.30, 3.2]	0.50	0
VIC	0.92 [0.81, 1.1]	0.17	1.3 [1.04, 1.7]	0.97	651
WA	1.26 [1.09, 1.5]	0.99	1.3 [0.67, 2.6]	0.80	0

Figure 5: Depiction of the relationship between R_{eff} analysis components. TTD = time from symptom onset to detection.

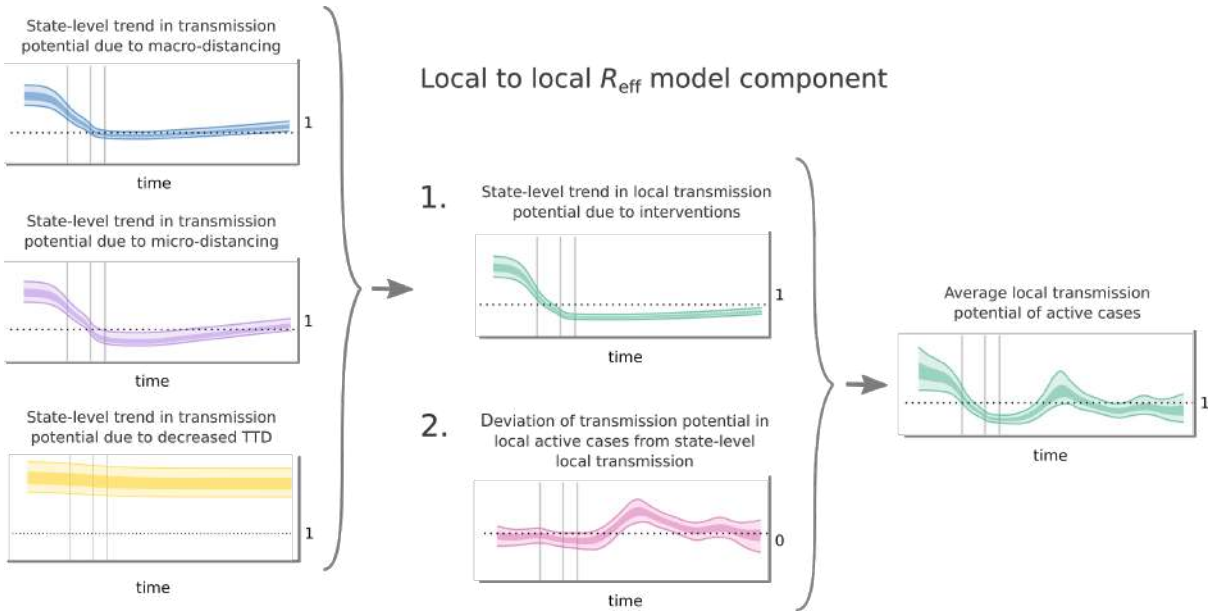

Figure 6: Estimate of local transmission potential averaged over state/territory population (Component 1); *i.e.*, removing short-term variation due to clusters (Component 2). Light green ribbon=90% credible interval; dark green ribbon = 50% credible interval. Estimates are made up to 1 July, based on cases with inferred infection dates up to and including 1 July. Solid grey vertical lines indicate key dates of implementation of various physical distancing policies. This includes the combined effect of macro- and micro-distancing behaviours and surveillance measures.

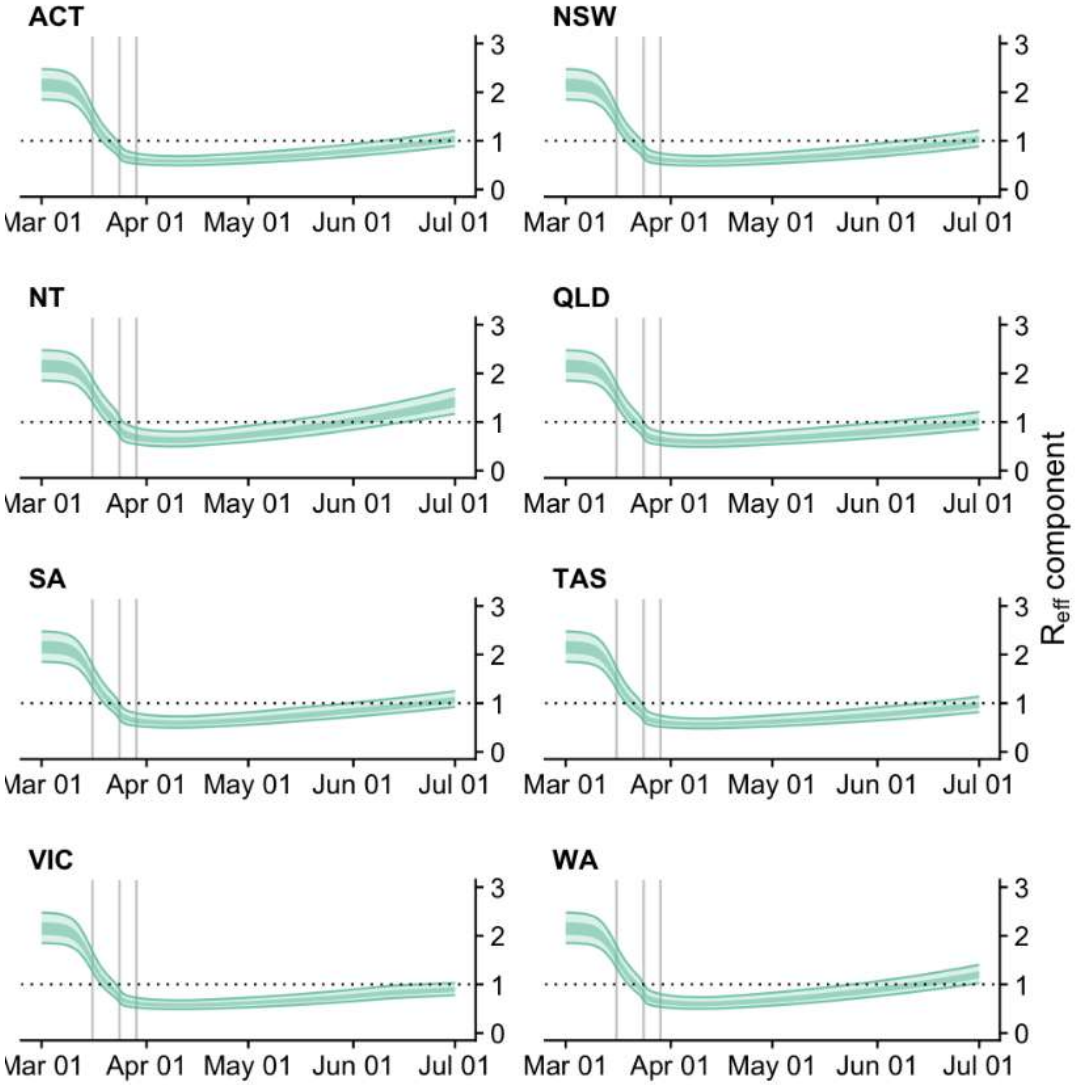

Figure 7: Deviation of transmission potential in local active cases (*e.g.*, clusters) from state-level local transmission potential (Component 2) for each state/territory (light pink ribbon=90% credible interval; dark pink ribbon = 50% credible interval. Estimates are made up to 1 July based on cases with inferred infection dates up to and including 1 July (due to a delay from infection to reporting, the trend in estimates after 1 July reflects the average range of deviations for that state, indicated by the grey shading). Solid grey vertical lines indicate key dates of implementation of various physical distancing policies.

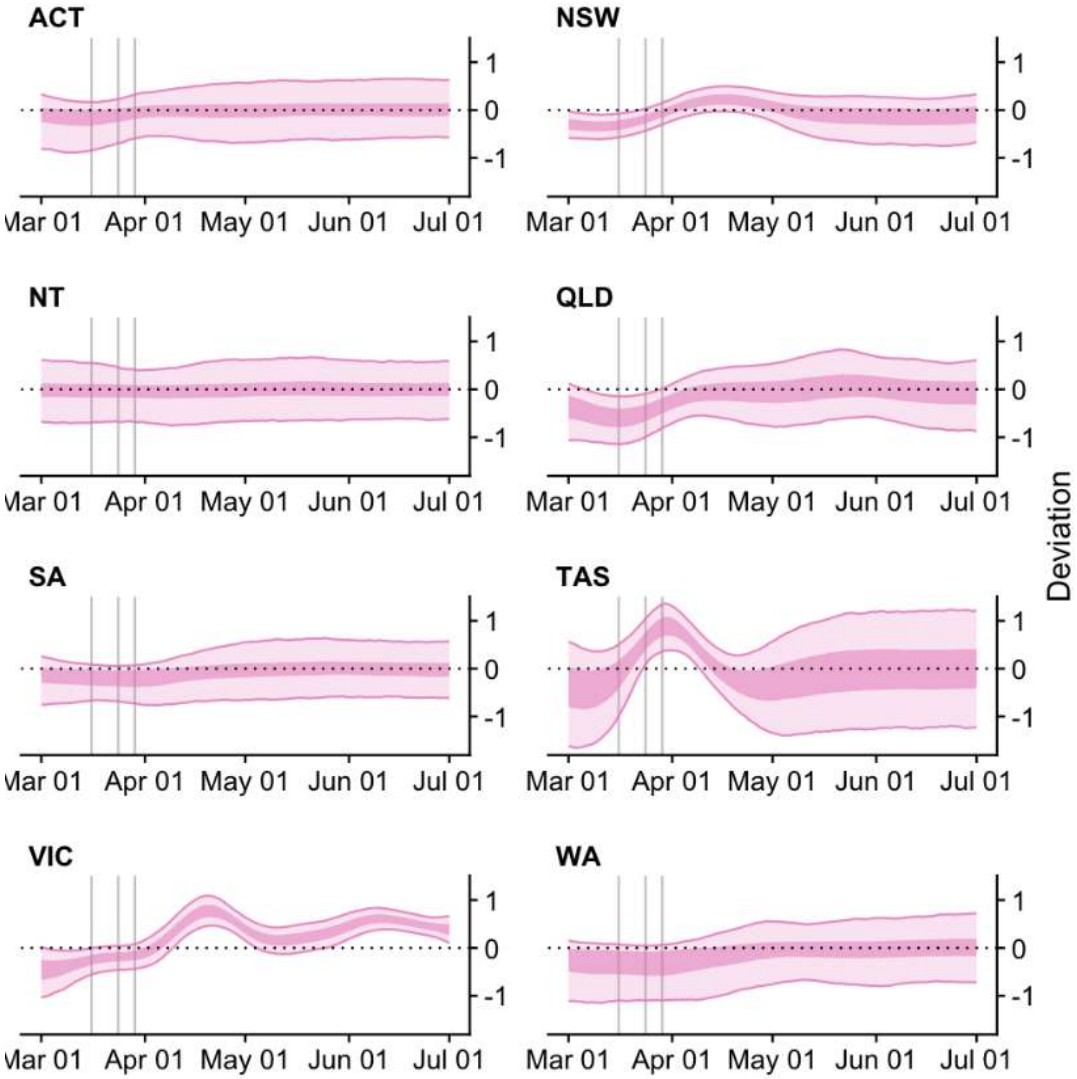

Figure 8: Estimate of average local transmission potential of active cases (Component 1&2) for each state/territory (light green ribbon=90% credible interval; dark green ribbon = 50% credible interval). Estimates are made up to 1 July based on cases with inferred infection dates up to and including 1 July (due to a delay from infection to reporting, the trend in estimates after 1 July is inferred from mobility data, indicated by the grey shading). Solid grey vertical lines indicate key dates of implementation of various physical distancing policies. Black dotted line indicates the target value of 1 for the effective reproduction number required for control. Where there is epidemic activity, this quantity may be interpreted as the effective reproduction number, R_{eff}. In the absence of epidemic activity, this quantity reflects the ability for the virus, if it were present, to establish and maintain community transmission (> 1) or otherwise (< 1).

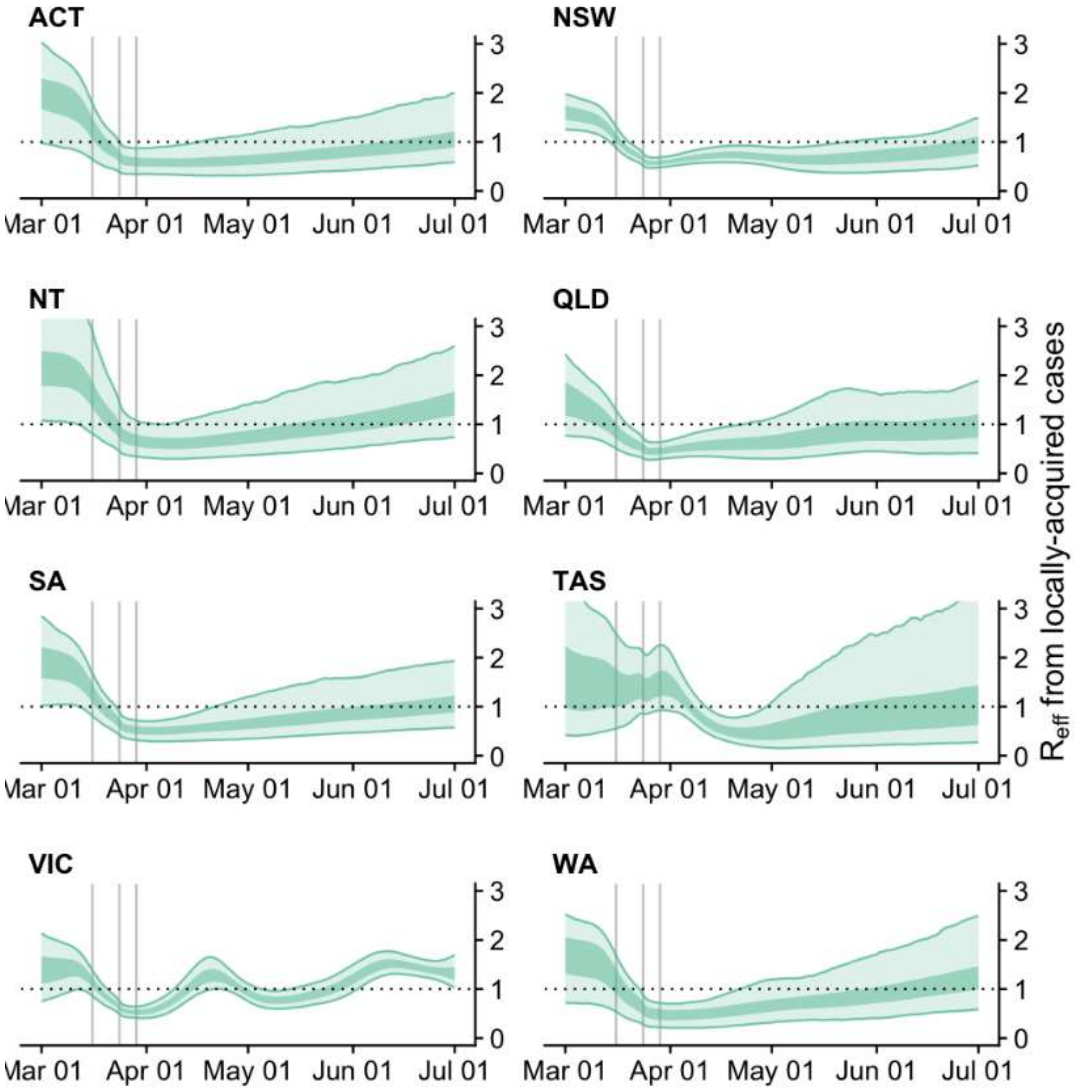

Forecasts of the daily number of new confirmed cases

We report forecasts of the daily number of new confirmed cases for each Australian state/territory up to 3 August— *synthesised* from three independent models (known as an 'ensemble forecast').

Ensemble forecasts are more accurate than any individual forecast alone — biases and variances in each model that result from different modelling choices balance against each other to improve predictions. Hence, ensemble forecasts tend to produce improved estimates of both the central values, as well as improved estimates of the plausible yet unlikely forecasts (uncertainty). Here, the ensemble has been generated by equally weighting the forecasts from each model. In future weeks, we will continue to improve the ensemble performance by updating the weights for each model based on their past-performance.

A brief description of each method incorporated in the ensemble is given below:

- **SEEIIR Forecast**: A stochastic susceptible-exposed-infectious-recovered (SEEIIR) compartmental model that incorporates changes in local transmission potential via the estimated time-varying effective reproduction number (as shown in Figure 8). Details can be found in our technical report at:
  `https://www.doherty.edu.au/about/reports-publications`.

- **Probabilistic Forecast**: A stochastic epidemic model that accounts for the number of imported-, symptomatic- and asymptomatic-cases over time. This model estimates the effective reproduction number corresponding to local and imported cases, and incorporates mobility data to infer the effect of macro-distancing behaviour. This model captures variation in the number and timing of new infections via probability distributions. The parameters that govern these distributions are inferred from the case and mobility data (*e.g.*, mean number of imported cases).

- **Time-Series Forecast**: A time-series model that does not account for disease transmission dynamics, but rather uses recent daily case counts to forecast cases into the future. Parameters of this 'autoregressive' model are estimated using global data accessible via the Johns Hopkins COVID-19 repository. Case counts from a specific time window prior to the forecasting date (the present) are used for model calibration. The number of days within this time window is chosen to optimise projections for Australian data.

The SEEIIR and Probabilistic Forecasts explicitly incorporate dynamics of disease transmission and the impact of public health measures on transmission over time via R_{eff}. The Time-Series Forecast does not explicitly incorporate either of these factors. The Time-Series Forecast is expected to accurately forecast new daily case numbers over a shorter time period, whereas disease-specific models are anticipated to provide more accurate forecasts several weeks into the future. All forecasts assume that current public health measures will remain in place and that public adherence to these measures will be consistent into the future.

Results

If local transmission potential remains at its current estimated level (as of 1 July), we anticipate that daily local case counts will remain very low or zero into August for all states/territories, except Victoria (Figures 9 and 10).

Forecasts for Victoria are highly uncertain at this time. Of the three models in the ensemble: the SEEIIR Forecast predicts a substantial increase in caseload into August, the Probabilistic

Forecast predicts a moderate increase, and the Time-Series Forecast suggests that a decrease is also plausible (Figure 11).

Note that the forecast for New South Wales does not take into account the spike in cases observed in early July which has resulted in an estimated R_{eff} of 1.28 [0.89, 1.82] as of 13 July. The forecast in this report no longer reflects our expectations of case loads for New South Wales into August, given that an outbreak has been seeded.

Forecasts of the daily number of new local cases for each state/territory

Figure 9: Time series of new daily local cases of COVID-19 estimated from the forecasting ensemble model for each jurisdiction (50–90% confidence intervals coloured in progressively lighter blue shading) from 6 July to 3 August. The observed daily counts of locally acquired cases are also plotted by date of symptom onset (grey bars). Recent case counts are inferred to adjust for reporting delays (black dots).

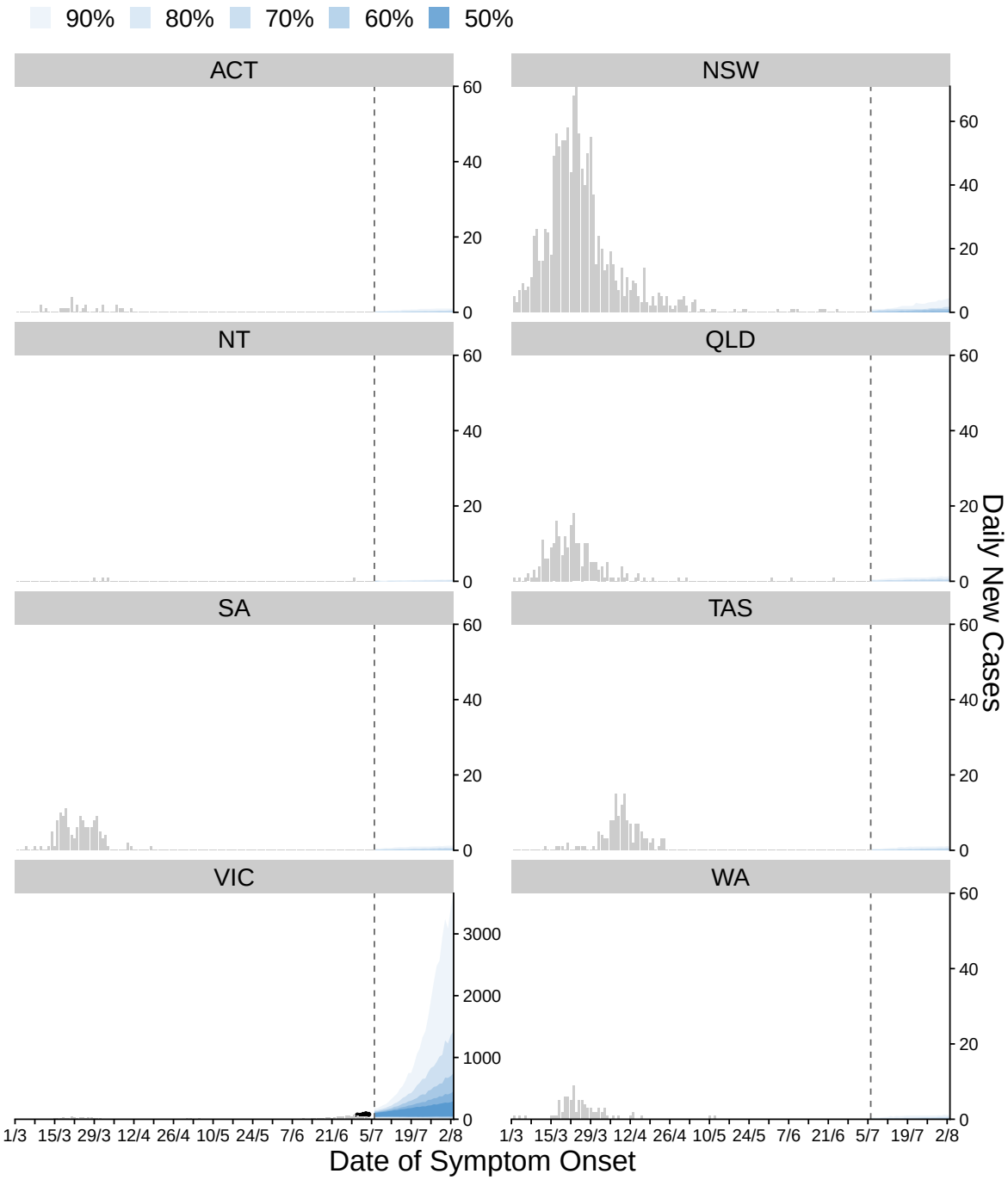

Figure 10: Time series of new daily local cases of COVID-19 estimated in Victoria from the forecasting ensemble model (50–90% confidence intervals coloured in progressively lighter blue shading) from 6 July to 3 August. Note that the y-axis is truncated at 1000 daily new cases (*i.e.*, zoomed in on lower projected cases counts). Recent case counts are inferred to adjust for reporting delays (black dots).

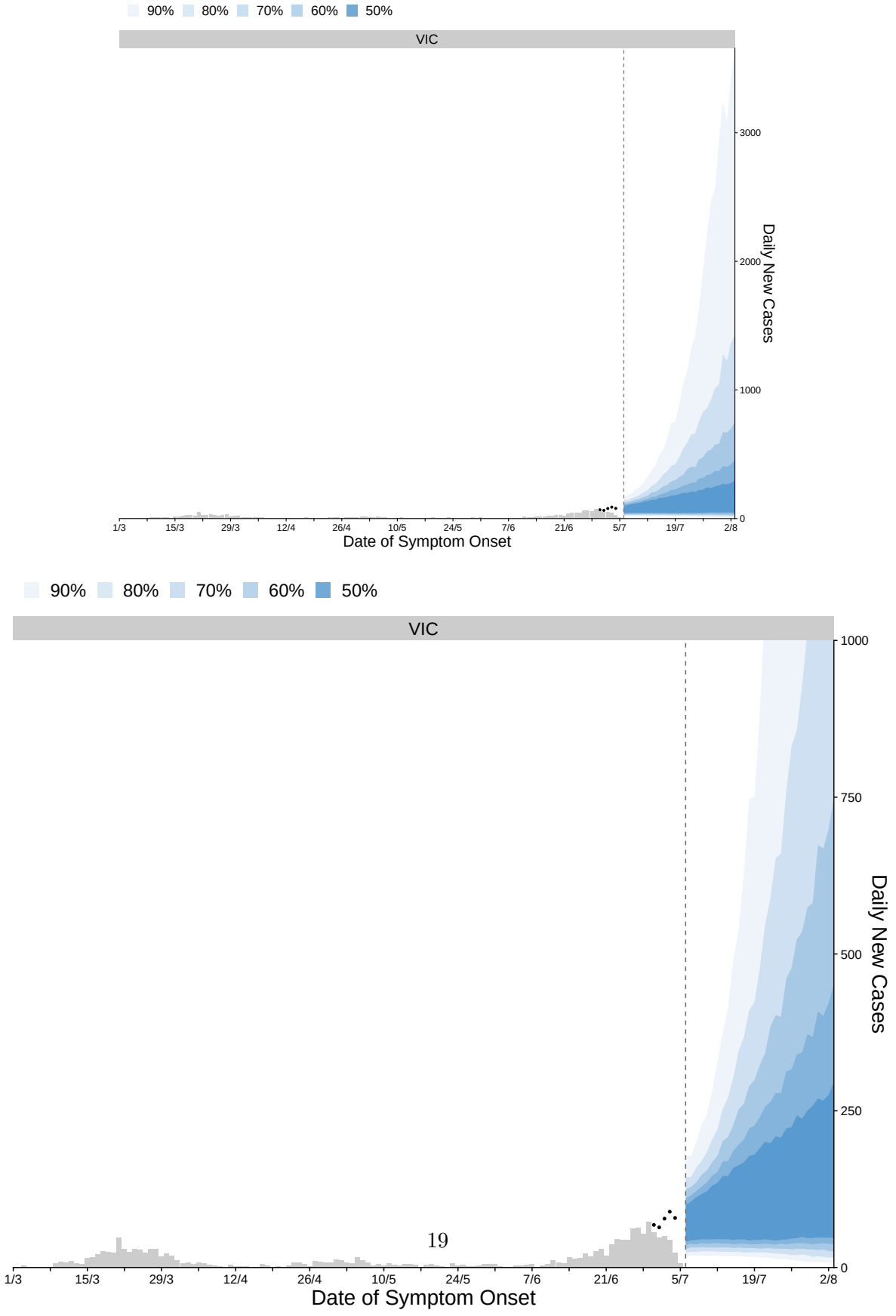

Figure 11: Panels show time series of new daily local cases of COVID-19 estimated in Victoria from the three forecasting models in the ensemble (50–90% confidence intervals coloured in progressively lighter shading), from 6 July to 3 August. Recent case counts are inferred to adjust for reporting delays (black dots).

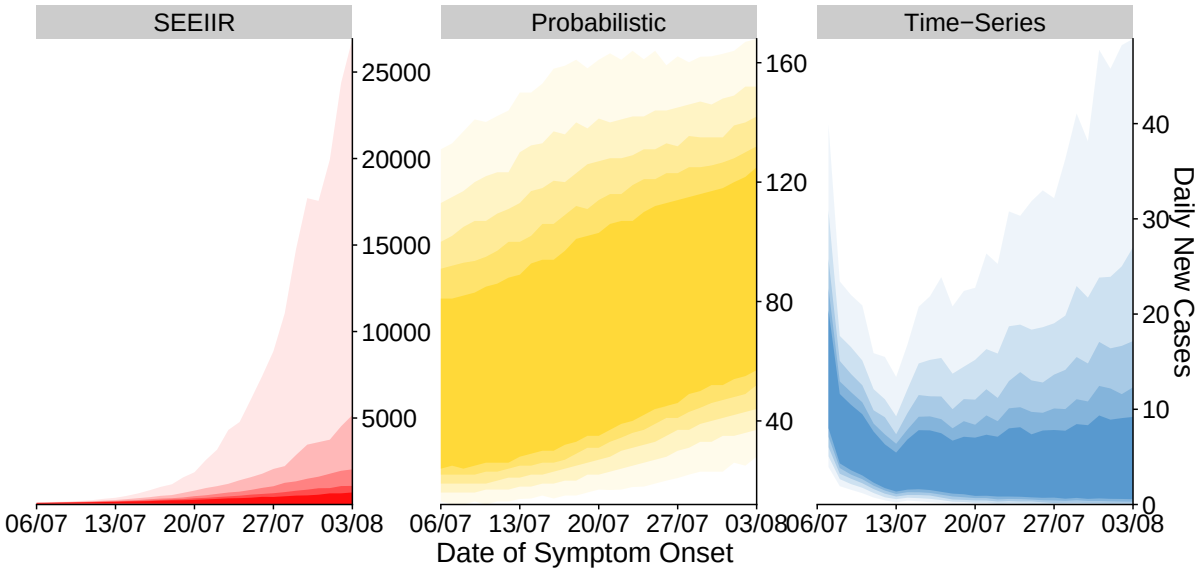

Forecasting alternate scenarios of the June outbreak in Victoria

A scenario analysis was performed to assess the potential impact of alternate scenarios on the Victorian outbreak. Estimates of the R_{eff} of local active cases for Victoria as of 1 July were projected forward through to 3 August for three alternate scenarios:

- Scenario 0: The forecast based on current estimates of local transmission potential
- Scenario 1: State-wide distancing behaviour returned to levels estimated on 13 May
- Scenario 2: State-wide distancing behaviour returned to peak levels of adherence (which is estimated to have occurred in Victoria on 13 April)
- Scenario 3: Overall public health response at peak level of impact (Component 2 of R_{eff} from 29 March and Component 1 of R_{eff} from 13 April)

Estimated values of R_{eff} up to 1 July and observed cases were then used as inputs into a mathematical model of transmission dynamics (specifically, the SEEIIR Forecast model). The model was projected forward from 4 July up to 3 August using the projected values of R_{eff} for each scenario to forecast the daily number of new cases in Victoria.

Results

If peak levels of transmission mitigation (Scenario 3) were achieved, this would result in a rapid decline in cases over the coming month (Figure 15). However, more likely is an intermediate effect (Scenario 1 or 2) in which control is achieved but with slowly declining epidemic activity over the next month (Figures 13 and 14). Note: even with improved transmission mitigation, epidemic growth is possible (upper credible intervals in Figures 13 and 14).

Because our model operates at the state-level, the appropriate interpretation of our results is that the enhanced distancing measures are geographically co-located with areas of high transmission. We note that this may not be the case due to both people's behaviour and the time delay between transmission activity and case reporting, leading to a mismatch between listed and actual areas of heightened transmission. Note: we plot observed and forecast infections by date of symptom onset, which differs from notification and reporting dates.

Figure 12: **Scenario 0**: Forecast of new daily local cases of COVID-19 estimated from the SEEIIR forecasting model (50–90% confidence intervals coloured in progressively lighter blue shading), from 4 July to 3 August, **based on current estimates of local transmission potential**. The observed daily counts of locally acquired cases are also plotted by date of symptom onset (grey bars).

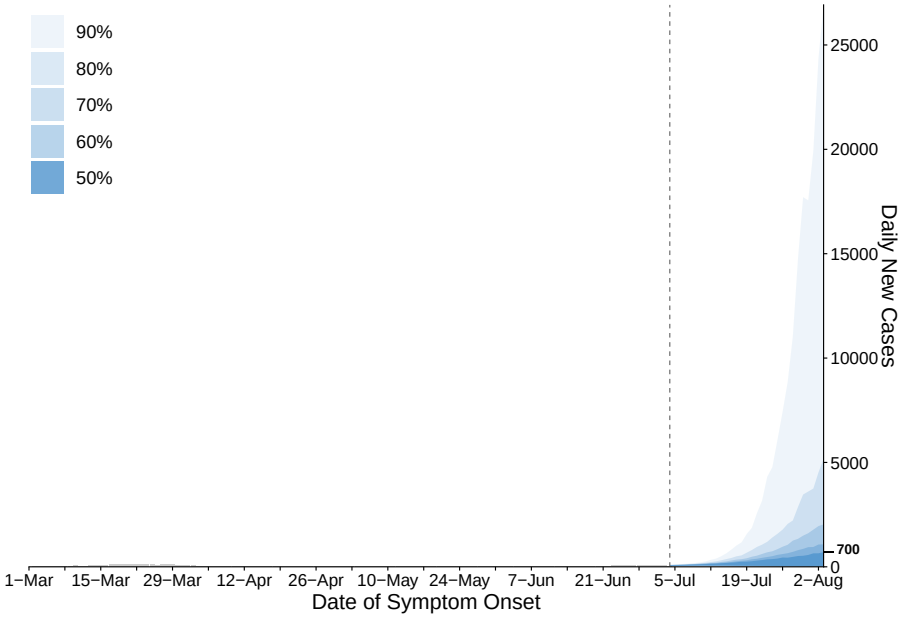

Figure 13: **Scenario 1**: Forecast of new daily local cases of COVID-19 estimated from the SEEIIR forecasting model, from 4 July to 3 August, **assuming that state-wide distancing behaviour returned to levels estimated on 13 May**. The observed daily counts of locally acquired cases are also plotted by date of symptom onset (grey bars).

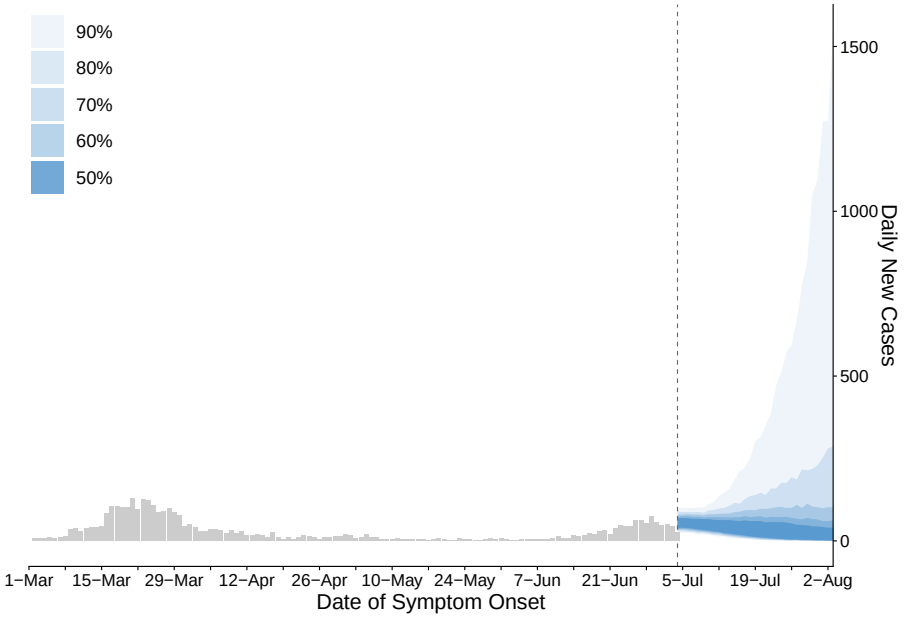

Figure 14: **Scenario 2**: Forecast of new daily local cases of COVID-19 estimated from the SEEIIR forecasting model (50–90% confidence intervals coloured in progressively lighter blue shading), from 4 July to 3 August, **assuming state-wide distancing behaviour returned to peak levels of adherence**. The observed daily counts of locally acquired cases are also plotted by date of symptom onset (grey bars).

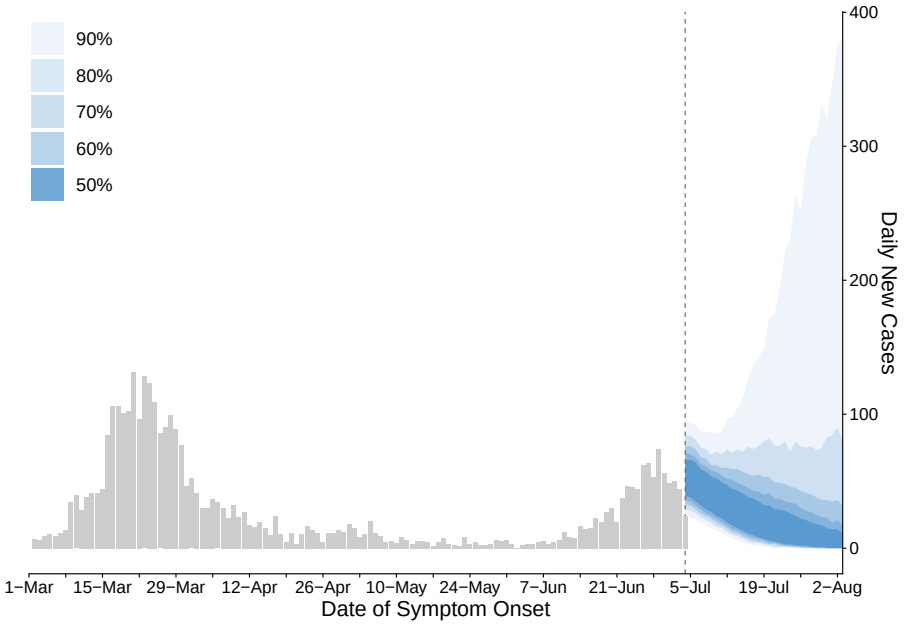

Figure 15: **Scenario 3**: Forecast of new daily local cases of COVID-19 estimated from the SEEIIR forecasting model (50–90% confidence intervals coloured in progressively lighter blue shading), from 4 July to 3 August, **assuming that the overall public health response returned to peak levels of impact**. The observed daily counts of locally acquired cases are also plotted by date of symptom onset (grey bars).

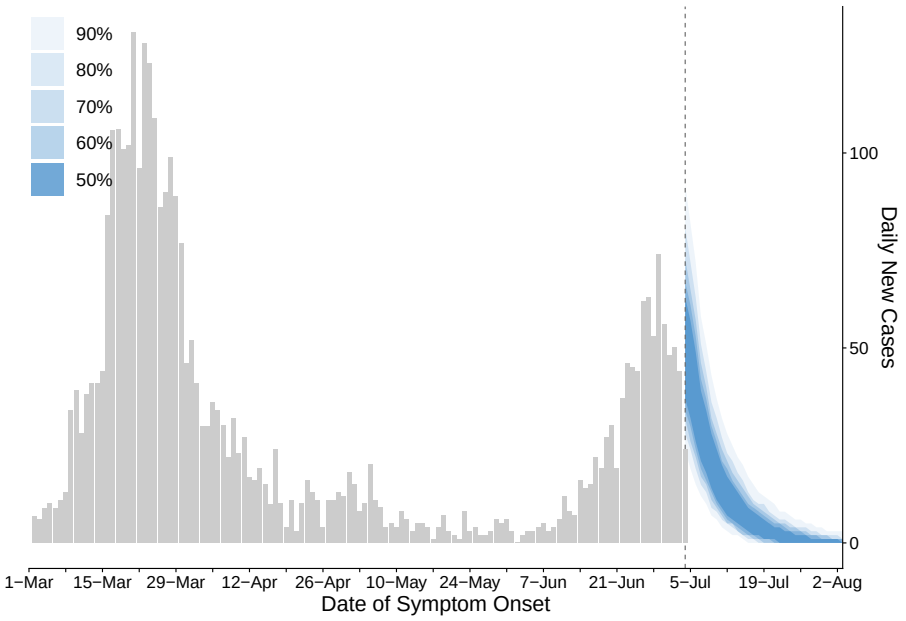

Acknowledgements

This report represents surveillance data reported through the Communicable Diseases Network Australia (CDNA) as part of the nationally coordinated response to COVID-19. We thank public health state from incident emergency operations centres in state and territory health departments, and the Australian Government Department of Health, along with state and territory public health laboratories. We thank members of CDNA for their feedback and perspectives on the results.

The report includes our analysis of survey data supplied by the Behavioural Economics Team of the Australian Government (BETA) in the Department of the Prime Minister and Cabinet. We thank members of the BETA team for this collaboration.

Supplementary Appendix

For full methodological details on the population mobility analysis, please refer to our previous Technical Report (dated 15 May 2020) available at the following link:

`https://www.doherty.edu.au/about/reports-publications`

Supplement: model of local transmission potential

Overview

We developed a new model to estimate components of the effective reproduction number resulting from transmission from locally acquired cases and from overseas acquired cases. This model enables us to 1) estimate the relative temporal variation in transmission from local to local cases and from overseas-acquired to local cases and 2) quantify the relative impacts of national-level interventions on transmission in Australia. Whilst both locally and overseas acquired cases contribute to Australia's case count, the transmission rates from each of these groups differs as they are each targeted by different interventions. Quarantine of overseas arrivals modifies the transmission rates of overseas acquired cases only, and physical distancing measures modify transmission rates of locally acquired cases. By splitting R_{eff} between these two groups, the model enables us to estimate the relative impacts of various response policies on transmission in Australia, namely quarantine of overseas arrivals and physical distancing of the general population.

We model local to local transmission and import to local transmission for each state/territory using two components:

1. the **average state-level trend** in R_{eff} driven by interventions (specifically changes in macro- and micro-distancing behaviour over time and quarantine of overseas arrivals);
2. **short-term fluctuations** in R_{eff} in each state/territory to capture stochastic dynamics of transmission, such as clusters of cases and short periods of low transmission.

Modelling the impact of physical distancing

We model the impact of physical distancing on transmission, quantifying how key distancing behaviours have changed over time — informed by both surveys and mobility data — and using an epidemiological model to relate those changes to transmission. Specifically, we consider the average number of non-household contacts for the population of each state/territory over time (termed macro-distancing), and the proportion of those state populations adhering to hygienic behaviour (termed micro-distancing, and compliance with the '1.5m rule' as an indicator). The population mobility analysis reported in previous reports identified a common trend in all available data streams, whereby population mobility was reduced around the dates that three physical distancing restrictions were implemented. Both macro- and micro-distancing behaviours are assumed to have changed following the same temporal pattern. But since reaching their peak, both forms of distancing have subsequently waned, and it is unlikely that these are well reflected by any one mobility metric. Using nationally-representative surveys, we can directly estimate the levels of macro- and micro-distancing in each state and how they have changed over time. These macro- and micro-distancing trends inform how the average state-level trends in R_{eff} have changed, even in states where there are no longer any active cases. The resulting measures of transmission potential indicate how rapidly the disease could spread if re-introduced to those states/territories.

Modelling the impact of quarantine of overseas arrivals

We model the impact of quarantine of overseas arrivals via a 'step function' reflecting three different quarantine policies: self-quarantine of overseas arrivals from specific countries prior to March 15; self-quarantine of all overseas arrivals from March 15 up to March 27; and mandatory quarantine of all overseas arrivals after March 27 (Figure S1). We make no prior assumptions

about the effectiveness of quarantine at reducing R_{eff} import, except that each successive change in policy increased that effectiveness.

Figure S1: Nationwide average reduction in R_{eff} that is due to quarantine of overseas arrivals estimated from the R_{eff} model (light orange ribbon=90% credible interval; dark orange ribbon = 50% credible interval). Note that this trend does not capture time-varying fluctuations in R_{eff} in each state/territory. Solid grey vertical lines indicate key dates of implementation of key response policies. Black dotted line indicates the target value of 1 for the effective reproduction number required for control. Note: A simple but naïve upper bound on R_{eff} import can be computed by assuming that all locally acquired cases arose from imported cases, and therefore computing the ratio of the numbers of local and imported cases. This results in a maximum possible value of the average R_{eff} import of 0.57.

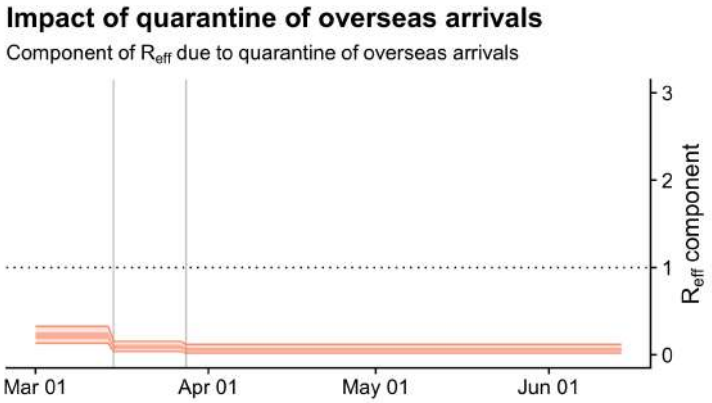

Model limitations

Note that while we have data on whether cases are locally acquired or overseas acquired, no data are currently available on whether each of the locally acquired cases were infected by an imported case or by another locally acquired case. This data would allow us to disentangle the two transmission rates. Without this data, we can separate the denominators (number of infectious cases), but not the numerators (number of newly infected cases) in each group at each point in time. The model we have developed enables us to estimate these effects from the currently available data but missing data reduces the precision of these estimates. For example, we currently cannot account for state-level variation in the impacts of quarantine of overseas arrivals or connect them to specific policies.

Should these data become available, this method will enable us to provide more precise estimates of R_{eff}.

Model description

We developed a semi-mechanistic Bayesian statistical model to estimate R_{eff}, or $R(t)$ hereafter, the effective rate of transmission of of SARS-CoV-2 over time, whilst simultaneously quantifying the impacts on $R(t)$ of a range of policy measures introduced at national and regional levels in Australia.

Observation model

A straightforward observation model to relate case counts to the rate of transmission is to assume that the number of new locally-acquired cases $N_i^L(t)$ at time t in region i is (conditional on its expectation) Poisson-distributed with mean $\lambda_i(t)$ given by the product of the total infectiousness of infected individuals $I_i(t)$ and the time-varying reproduction rate $R_i(t)$:

$$N_i^L(t) \sim \text{Poisson}(\lambda_i(t)) \tag{1}$$

$$\lambda_i(t) = I_i(t) R_i(t) \tag{2}$$

$$I_i(t) = \sum_{t'=0}^{t} g(t') N_i(t') \tag{3}$$

$$N_i(t') = N_i^L(t) + N_i^O(t) \tag{4}$$

where the total infectiousness, $I_i(t)$, is the sum of all active infections $N_i(t')$ — both locally-acquired $N_i^L(t')$ and overseas-acquired $N_i^O(t')$ — initiated at times t' prior to t, each weighted by an infectivity function $g(t')$ giving the proportion of new infections that occur t' days post-infection. The function $g(t')$ is the probability of an infector-infectee pair occurring t' days after the infector's exposure, *i.e.*, a discretisation of the probability distribution function corresponding to the generation interval.

This observation model forms the basis of the maximum-likelihood method proposed by White and Pagano (2007) [1] and the variations of that method by Cori et al. (2013) [**?**], Thompson et al. (2019) [2] and Abbott et al. (2020) [3] that have previously been used to estimate time-varying SARS-CoV-2 reproduction numbers in Australia.

We extend this model to consider separate reproduction rates for two groups of infectious cases, in order to model the effects of different interventions targeted at each group: those with locally-acquired cases $I_i^L(t)$, and those with overseas acquired cases $I_i^O(t)$, with corresponding reproduction rates $R_i^L(t)$ and $R_i^O(t)$. These respectively are the rates of transmission from imported cases to locals, and from locally-acquired cases to locals. We also model daily case counts as arising from a Negative Binomial distribution rather than a Poisson distribution to account for potential clustering of new infections on the same day, and use a time-varying generation interval distribution $g(t', t)$ (detailed in *Surveillance effect model*):

$$N_i^L(t) \sim \text{NegBinomial}(\mu_i(t), r) \tag{5}$$

$$\mu_i(t) = I_i^L(t) R_i^L(t) + I_i^O(t) R_i^O(t) \tag{6}$$

$$I_i^L(t) = \sum_{t'=0}^{t} g(t, t') N_i^L(t) \tag{7}$$

$$I_i^O(t) = \sum_{t'=0}^{t} g(t,' t) N_i^O(t) \tag{8}$$

where the negative binomial distribution is parameterised in terms of its mean $\mu_i(t)$ and dispersion parameter r. In the commonly used probability and dispersion parameterisation with probability ψ the mean is given by $\mu = \psi r/(1-\psi)$.

Note that if data were available on the whether the source of infection for each locally-acquired case was another locally-acquired case or an overseas-acquired cases, we could split this into two separate analyses using the observation model above; one for each transmission source. In the absence of such data, the fractions of all transmission attributed to sources of each type is implicitly inferred by the model, with an associated increase in parameter uncertainty.

Reproduction rate models

We model the reproduction rates for overseas-acquired and locally-acquired cases in a semi-mechanistic way. Both reproduction rates are modelled as the product of a deterministic model of the population-wide transmission potential for that type of case, and a correlated time series of random effects to represent stochastic fluctuations in the reporting rate in each state over time:

$$R_i^L(t) = R_i^*(t)e^{\epsilon_i^L(t)} \tag{9}$$

$$R_i^O(t) = R_i^*(0)Q(t)e^{\epsilon_i^O(t)} \tag{10}$$

For locally-acquired cases, the state-wide average transmission rate at time t, $R_i^*(t)$, is given by a deterministic epidemiological model of population-wide transmission potential that considers the effects of distancing behaviours. For overseas-acquired cases the population-wide transmission rate at time t, $R_i^*(0)Q(t)$, is the baseline rate of transmission ($R_i^*(0) = R_0$; local-local transmission potential in the absence of distancing behaviour or other mitigation) multiplied by a quarantine effect model, $Q(t)$, that encodes the efficacy of the three different overseas quarantine policies implemented in Australia (described below). The correlated time series of random effects $\epsilon_i^L(t)$ and $\epsilon_i^O(t)$ represent stochastic fluctuations in these transmission rates in each state. For overseas-acquired cases, $\epsilon_i^O(t)$ represents any interstate-differences or temporal variations in quarantine effectiveness that are not explained by the model of national policy. For locally-acquired cases $\epsilon_i^L(t)$ represents stochastic fluctuations in the reproduction rate among active cases at each point in time — for example due to clusters of transmission in sub-populations with higher or lower reproduction rates than the general population.

We model $R_i^*(t)$, the population-wide rate of local-local transmission at time t, as the sum of two components: the rate of transmission to members of the same household, and to members of other households. Each of these components is computed as the product of the number of contacts, and the probability of transmission per contact. The transmission probability is in turn modelled as a binomial process considering the duration of contact with each person and the probability of transmission per unit time of contact. This mechanistic consideration of the contact process enables us to separately quantify how macro- and micro-distancing behaviours impact on transmission, and to make use of various ancillary measures of both forms of distancing:

$$R_i^*(t) = s(t)(HC_0(1-(1-p)^{HD_0h_i(t)d}) + NC_0\delta_i(t)d(1-(1-p)^{ND_0})\gamma_i(t)) \tag{11}$$

where $s(t)$ is the effect of surveillance on transmission, due to the detection and isolation of cases (detailed below), HC_0 and NC_0 are the baseline (*i.e.*, before adoption of distancing behaviours) daily rates of contact with, respectively, people who are, and are not, members of the same household, HD_0 and ND_0 are the baseline average total daily duration of contacts with household and non-household members (measured in hours), d is the average duration of infectiousness in days, p is the probability of transmitting the disease per hour of contact, $h_i(t)$, $\delta_i(t)$, $\gamma_i(t)$ are time-varying indices of change relative to baseline of: the duration of household contacts, the number of non-household contacts, and the transmission probability per non-household contact; (modifying both the duration and transmission probability per unit time for non-household contacts).

The first component in equation (11) is the rate of household transmission, and the second is the rate of non-household transmission. Note that the duration of infectiousness d is considered differently in each of these components. For household members, the daily number of household contacts is typically close to the total number of household members, hence the

expected number of household transmissions saturates at the household size; so the number of days of infectiousness contributes to the probability of transmission to each of those household members. This is unlikely to be the case for non-household members, where each day's non-household contacts may overlap, but are unlikely to be from a small finite pool. This assumption would be unnecessary if contact data were collected on a similar timescale to the duration of infectiousness, though issues with participant recall in contact surveys mean that such data are unavailable.

The parameters HC_0, HD_0, and ND_0 are all estimated from a contact survey conducted in Melbourne in 2015 [4]. NC_0 is computed from an estimate of the total number of contacts per day for adults from [5], minus the estimated rate of household contacts. Whilst [4] also provides an estimate of the rate of non-household contacts, the method of data collection (a combination of 'individual' and 'group' contacts) makes it less comparable with contemporary survey data than the estimate of [5].

The expected duration of infectiousness d is computed as the mean of the discrete generation interval distribution:

$$d = \sum_{t'=0}^{\infty} t' g(t, t') \tag{12}$$

and change in the duration of household contacts over time $h_i(t)$ is assumed to be equivalent to change in time spent in residential locations in state i, as estimated by the mobility model for the data stream *Google: time at residential*. In other words, the total duration of time in contact with household members is assumed to be directly proportional to the amount of time spent at home. Unlike the effect on non-household transmission, an increase in macro-distancing is expected to slightly increase household transmission due to this increased contact duration.

The time-varying parameters $\delta_i(t)$ and $\gamma_i(t)$ respectively represent macro- and micro-distancing; behavioural changes that reduce mixing with non-household members, and the probability of transmission for each of non-household member contact. We model each of these components, informed by population mobility estimates from the mobility model and calibrated against data from nationwide surveys of contact behaviour.

Surveillance effect model

Disease surveillance — both screening of people with COVID-like symptoms and performing contact tracing — can improve COVID-19 control by placing cases in isolation so that they are less likely to transmit the pathogen to other people. Improvements in disease surveillance can therefore lead to a reduction in transmission potential by isolating cases more quickly, and reducing the time they are infectious but not isolated. Such an improvement changes two quantities: the population average transmission potential $R^*(t)$ is reduced by a constant rate $s(t)$; and the generation interval distribution $g(t, t')$ is shortened, as any transmission events are more likely to occur prior to isolation.

We model both of these functions using a time-varying estimate of the discrete probability

distribution over times from infection to detection $f(t,t')$:

$$g(t,t') = \frac{f(t,t')g^*(t')}{s(t)} \tag{13}$$

$$s(t) = \sum_{t'=0}^{\infty} f(t,t')g^*(t') \tag{14}$$

$$f(t,t') = \begin{cases} 0 & t' < 3 \\ q(t)/2 & 3 \geq t' < 5 \\ (1-q(t))F(t,t') & t' \geq 5 \end{cases} \tag{15}$$

$$F(t,t') = \text{NegBinomial}(t'-5|\mu_f(t), r_f) \tag{16}$$

where $g^*(t')$ is the baseline generation interval distribution, representing times to infection in the absence of detection and isolation of cases, $s(t)$ is a normalising factor, and $f(t,t')$ is modelled as a two-stage hurdle model, where the probability of detection: prior to 3 days post-infection is zero (insufficient virus would be present to be detected); over the next two days has a constant probability, and; over each of the subsequent days is equivalent to the probability mass function of a negative binomial distribution over $t'-5$. Symptom onset is assumed to be exactly 5 days subsequent to infection, so the time since infection t' is converted to the time since symptom onset, $t'-5$, allowing for the time from symptom onset to detection to be up to 5 days negative.

We used point estimates of probability masses $q(t)$ and $F(t,t')$ for all t and values of t' in $\{0,1,\ldots,20\}$, computed as the posterior means of a Bayesian statistical model that was fitted in a separate modelling step (to observed times τ_i from symptom onset to first specimen collection of locally-acquired cases with dates of infection t_i). Specimen collection was deemed the most indicative of the date of isolation, since patients are typically advised to self-isolate once they are considered a suspected case until they receive a test result, reducing their ability to transmit. The model was fitted as a two-step hurdle model, with a parameter for the probability of a negative τ_i, and parameters for a negative binomial count distribution over non-negative τ_i:

$$y_i = \begin{cases} 1 & t'_i < 0 \\ 0 & t'_i \geq 0 \end{cases} \tag{17}$$

$$y_i \sim \text{Bernoulli}(q(t_i)) \tag{18}$$

$$t'_j \sim \text{NegBinomial}(\mu_f(t_j), r_f) \tag{19}$$

$$\text{logit}(q(t_i)) = \alpha_q + \beta_q z(t_i) \tag{20}$$

$$\log(\mu_f(t_j)) = \alpha_f + \beta_f z(t_j) \tag{21}$$

$$\text{logit}(z(t_i)) = \beta_z(t_i - \mu_z) \tag{22}$$

where y_i is an indicator for whether t'_i is negative, j indexes only the positive elements of t' (i.e. $y_j = 0$), the logit-probability of a negative time (equation (20)) and the log-mean of non-negative times (equation (21)) are both modelled as linear functions of the same latent factor, $z(\cdot)$, itself a sigmoidal or logistic function of time with inflection time μ_z, and rate of change β_z. We assume that any recorded values of $t_i < -2$ are erroneously recorded, and must represent a date of symptom onset no more than two days later than a positive test result. In practice, these are rare, so this assumption has negligible impact on the model.

Macro-distancing model

The population-wide average daily number of non-household contacts at a given time can be

directly estimated using a contact survey. We therefore used data from a series of contact surveys commencing immediately after the introduction of distancing restrictions to estimate $\delta_i(t)$ independently of case data. To infer a continuous trend of $\gamma_i(t)$, we model the numbers of non-household contacts at a given time as a function of mobility metrics considered in the mobility model. We use the model estimated trend in five Google metrics of time spent at different types of location: residential, transit stations, parks, workplaces, and retail and recreation. We use data on the proportion of contacts in the baseline contact survey [4] that took place at each of these location types to form a prior distribution over a column vector of weights ω, which are used to combine these five mobility metrics into a single metric of the relative change in numbers of contacts. We then multiply this index of relative change by a scaling parameter α to give the absolute rate of change in non-household contacts from the baseline value:

$$\delta_i(t) = (\omega \mathbf{M}_i(t))^\alpha \tag{23}$$

where $\mathbf{M}_i(t)$ is a row vector of the estimated values of the five Google mobility indices in state i at time t.

We estimate the parameters ω and α using a Bayesian model with negative binomial likelihood over $NC_{i,j,t}$, the number of non-household contacts reported by contact survey respondent j in state i in the survey wave commencing at time t:

$$NC_i(t) \sim \text{NegBinomial}(\mu_i(t), r_{NC}) \tag{24}$$

$$\mu_i(t) = NC_0 \delta_i(t) \tag{25}$$

where the negative binomial is parameterised as described above, and r_{NC} is the dispersion parameter.

Micro-distancing model

Unlike with macro-distancing behaviour and contact rates, there is no simple mathematical framework linking change in micro-distancing behaviours to changes in non-household transmission probabilities. We must therefore estimate the effect of micro-distancing behaviour on transmission via case data. We implicitly assume that any reduction in local-to-local transmission that is not explained by changes to the numbers of non-household contacts or the duration of household contacts, is explained by the effect of micro-distancing on non-household transmission probabilities.

Whilst it is not necessary to use ancillary data to estimate the effect that micro-distancing has at its peak, we use behavioural survey data to estimate the temporal trend in micro-distancing behaviour, in order to estimate to what extent adoption of that behaviour has waned and how that has affected transmission potential.

We therefore model γ_t as a function of the proportion of the population adhering to micro-distancing behaviours. We consider adherence to the 1.5m rule as indicative of this broader suite of behaviours due to the availability of data on this behaviour in a weekly series of behavioural survey beginning prior to the last distancing restriction being implemented [**?**]. We consider the number $m^+_{i,t}$ of respondents in state i on survey wave commencing at time t replying that they 'always' keep 1.5m distance from non-household members, as a binomial sample with sample size $m_{i,t}$. We model $c_i(t)$, the proportion of the population in state i responding that they always comply as a function of time, composed of an initial adoption phase, a date of peak compliance, and a subsequent linear decrease in the rate of adoption. We assume that the temporal pattern in the initial rate of adoption of the behaviour is the same as for macro-distancing behaviours — the adoption curve estimated from the mobility model. In other words, we assume that all macro- and micro-distancing behaviours were adopted simultaneously. However we do not

assume that these behaviours peaked at the same time or waned at the same rate. The model for the proportion complying with this behaviour is therefore:

$$m^+_{i,t} = \text{Binomial}(m_{i,t}, c_i(t)) \tag{26}$$

$$c_i(t) = d_i(t)\kappa_{1,i} - w_i(t)\kappa_{2,i} \tag{27}$$

$$w_i(t) = \begin{cases} 0 & t < \kappa_0 \\ (t-\kappa_0)/(T-\kappa_0) & t \geq \kappa_0 \end{cases} \tag{28}$$

$$logit(\kappa_{1,i}) \sim N(\mu_{\kappa_1}, \sigma^2_{\kappa_1}) \tag{29}$$

$$logit(\kappa_{2,i}) \sim N(\mu_{\kappa_2}, \sigma^2_{\kappa_2}) \tag{30}$$

where $d_i(t)$ is the latent function for adoption of distancing behaviour, estimated from the mobility model (scaled from 0 at baseline to 1 at maximum), κ_0 is the time of peak compliance, $\kappa_{1,i}$ is the proportion in state i complying at peak, and $\kappa_{2,i}$ is the proportion in state i complying at time T, the most recent time for which data are available. Each $\kappa_{1,i}$ and $\kappa_{2,i}$ is drawn from a hierarchical distribution over states, enabling states to differ in the peak proportion complying and in the rate of waning, but sharing information between states. Given $c_i(t)$, we model $\gamma_i(t)$ as a function of the degree of micro-distancing relative to the peak:

$$\gamma_i(t) = 1 - \beta(c_i(t)/\kappa_{1,i}) \tag{31}$$

with β inferred from case data in the main R_{eff} model.

Overseas quarantine model

We model the effect of overseas quarantine $Q(t)$ via a monotone decreasing step function with values constrained to the unit interval, and with steps at the known dates τ_1 and τ_2 of changes in quarantine policy:

$$Q(t) = \begin{cases} q_1 & t < \tau_1 \\ q_2 & \tau_1 \leq t < \tau_2 \\ q_3 & \tau_2 \leq t \end{cases} \tag{32}$$

where $q_1 > q_2 > q_3$ and all parameters are constrained to the unit interval.

Error models

The correlated time series of errors in the log of the effective reproduction rate for each group $\epsilon^L_i(t)$ and $\epsilon^O_i(t)$ are each modelled as a zero-mean Gaussian process (GP) with covariance structure reflecting temporal correlation in errors within each state, but independent between states. We use a squared exponential covariance function k_{SE} for $\epsilon^O_i(t)$, reflecting the fact that any temporally-correlated fluctuations in quarantine effectiveness are likely to be comparatively smooth. For $\epsilon^L_i(t)$ we use a rational quadratic covariance function k_{RQ}, enabling periods of comparatively smooth variations, with occasional more rapid fluctuations, to represent the sudden rapid growth of cases that can occur with a high-transmission cluster. For both $\epsilon^L_i(t)$ and $\epsilon^O_i(t)$, parameters l_1, l_2 and α_2 which control the temporal range of correlation are assumed to be the same across states, whilst the magnitude of the deviations can differ between states, with a hierarchical structure:

$$\epsilon_i^O \sim GP(\mathbf{0}, k_{i,SE}(t,t')) \tag{33}$$

$$\epsilon_i^L \sim GP(\mathbf{0}, k_{i,RQ}(t,t')) \tag{34}$$

$$k_{i,SE}(t,t') = \sigma_1^2\,\sigma_{i,1}^2\,\exp\left(-\frac{(t-t')^2}{2l_1^2}\right) \tag{35}$$

$$k_{i,RQ}(t,t') = \sigma_2^2\,\sigma_{i,2}^2\,\exp\left(1+\frac{(t-t')^2}{2\alpha l_2^2}\right)^{-\alpha_2} \tag{36}$$

Components of local transmission potential
We model the rate of transmission from locally acquired cases as the product of the time-varying mechanistic model of transmission rates $R_i^*(t)$, and a temporally-correlated error term $e^{\epsilon_i^L(t)}$. This structure enables inference of mechanistically interpretable parameters whilst also ensuring that statistical properties of the observed data are represented by the model. Moreover, these two parts of the model can also be interpreted in epidemiological terms as two different components of transmission rates:

1. **Component 1** – transmission rates averaged over the whole state population, representing how macro- and micro-distancing affect the potential for widespread community transmission. ($R_i^*(t)$), and
2. **Component 2** – the degree to which the transmission rates of the population of current active cases deviates from the average statewide transmission rate ($e^{\epsilon_i^L(t)}$).

Component 2 reflects the fact that the population of current active cases in each state at a given time will not be representative of the the state-wide population, and may be either higher (*e.g.* when cases arise from a cluster in a high-transmission environment) or lower (*e.g.* when clusters are brought under control and cases placed in isolation).

Component 1 can therefore be interpreted as the expected rate of transmission if cases were widespread in the community. The product of Components 1 and 2 can be interpreted as the rate of transmission in the sub-population making up active cases at a given time.

Where a state has active cases in one or more clusters, the product of these components gives the apparent rate of transmission in those clusters. Where a state has no active cases, the product of Components 1 and 2 gives the rate of spread expected if an index case were to occur in a random sub-population. Because the amplitude of this error term is learned from the data, this is informative as to the range of plausible rates of spread that might be expected from a case being introduced into a random sub-population.

Parameter values and priors
Tables S1 and S3 give the prior distributions of parameters in the semi-mechanistic and time-series (ϵ^L and ϵ^O) parts of the model respectively. Table S2 gives fixed parameter values used in the semi-mechanistic part of the model.

The parameters of the generation interval distribution are the posterior mean parameter estimates corresponding to a Lognormal distribution over the serial interval estimated by [6]. The shape of the generation interval distribution for SARS-CoV-2 in comparable populations is not well understood, and a number of alternative distributions have been suggested by other analyses. A sensitivity analysis performed by running the model with alternative generation interval distributions (not presented here) showed that parameter estimates were fairly consistent between these scenarios, and the main findings were unaffected. A full, formal analysis of sensitivity to this and other assumptions will be presented in a future publication.

No ancillary data are available to inform p, the probability of transmission per hour of contact in the absence of distancing behaviour. However at $t = 0$, holding HC_0, NC_0 HD_0, and ND_0 constant, there is a deterministic relationship between p and $R_i^*(0)$ (the basic reproduction rate, which is the same for all states). The parameter p is therefore identifiable from transmission rates at the beginning of the first epidemic wave in Australia. We define a prior on p that corresponds to a prior over $R_i^*(0)$ matching the averages of the posterior means and 95% credible intervals for 11 European countries as estimated by [7] in a sensitivity analysis where the mean generation interval was 5 days — similar to the serial interval distribution assumed here. This corresponds to a prior mean of 2.79, and a standard deviation of 1.70 for $R_i^*(0)$. This prior distribution over p was determined by a Monte-Carlo moment-matching algorithm, integrating over the prior values for HC_0, NC_0 HD_0, and ND_0.

Model fitting

We fitted (separate) models of $c_i(t)$ and $NC_0\delta_i(t)$ to survey data alone in order to infer trends in those parameters as informed by survey data. These are shown in Figures 1–2. In order to incorporate those fitted trends into the R_{eff} model whilst ensuring uncertainty in the trends was fully accounted for, we re-fitted these models within the R_{eff} model, with a joint likelihood. That is, the likelihood of the R_{eff} model was the product of the likelihood for case data, and the two likelihoods for macro- and micro-distancing survey data. This is equivalent to incorporating the posterior distributions over $c_i(t)\kappa_{1,i}$ and $NC_0\delta_i(t)$ from the survey-data-only models as priors over those parameters in the R_{eff} model, but without the loss of information incurred by approximating the posteriors with some analytical distribution.

Inference was performed by Hamiltonian Monte Carlo using the R packages `greta` and `greta.gp` [8, 9]. Posterior samples of model parameters were generated by 10 independent chains of a Hamiltonian Monte Carlo sampler, each run for 1000 iterations after an initial, discarded, 'warm-up' period (1000 iterations per chain) during which the sampler step size and diagonal mass matrix was tuned, and the regions of highest density located. Convergence was assessed by visual assessment of chains, ensuring that the potential scale reduction factor for all parameters had values less than 1.1, and that there were at least 1000 effective samples for each parameter.

Visual posterior predictive checks were performed to ensure that the observed data fell within the posterior predictive density over all cases (and survey results), and over time-varying case predictions within each state.

Table S1: Parameters in the semi-mechanistic part of the time-varying model of R_{eff}. Prior on weights for ω correspond to Google mobility metrics in the following order: parks, residential, retail and recreation, transit stations, workplaces.

Prior distribution	Parameter description
$r^{-1/2} \sim \text{N}^+(0, 0.5)$	Overdispersion of observed daily new infections
$\text{logit}(p) \sim \text{N}(2.57, 0.08^2)$	Transmission probability per hour contact time
$HC_0 \sim \text{N}^+(2.09, 0.06^2)$	Baseline average daily household contacts
$NC_0 \sim \text{N}^+(10.70, 0.28^2)$	Baseline average daily non-household contacts
$HD_0 \sim \text{N}^+(1.05, 1.68^2)$	Baseline daily duration per household contact (hours)
$ND_0 \sim \text{N}^+(0.687, 0.05^2)$	Baseline daily duration per non-household contact (hours)
$\omega \sim \text{Dir}([0.06, 0.06, 0.27, 0.07, 0.19])$	Mobility-metric weights for non-household contact rates
$\alpha \sim \text{lognormal}(0, 1)$	Effect of weighted mobility on non-household contact rates
$r_{NC}^{-1/2} \sim \text{N}^+(0, 0.5)$	Overdispersion of daily non-household contacts
$\kappa_0 \sim \text{N}(\tau_3, T - \tau_3)[\tau_3, T]$	Timing of peak microdistancing (truncated)
$\mu_{\kappa_1} \sim \text{N}(0, 10^2)$	Hierarchical mean for state i microdistancing peak effect
$\sigma_{\kappa_1} \sim \text{N}^+(0, 0.5^2)$	Hierarchical s.d. for state i microdistancing peak effect
$\mu_{\kappa_2} \sim \text{N}(0, 10^2)$	Hierarchical mean for state i microdistancing waning
$\sigma_{\kappa_2} \sim \text{N}^+(0, 0.5^2)$	Hierarchical s.d. for state i microdistancing waning
$\beta \sim \text{U}(0, 1)$	Microdistancing effect on transmission
$q_1 \sim \text{U}(0, 1)$	Effect of quarantine of overseas arrivals (phase 1)
$q_2 \times q_1 \sim \text{U}(0, 1)$	Relative effect of quarantine (phase 2 vs 1)
$q_3 \times q_2 \sim \text{U}(0, 1)$	Relative effect of quarantine (phase 3 vs 2)

Table S2: Fixed parameters in the semi-mechanistic part of the time-varying model of R_{eff}.

Parameter value	Parameter description
$\tau_1 = 2020\text{-}03\text{-}15$	Date of change from arrivals policy phase 1 to 2
$\tau_2 = 2020\text{-}03\text{-}28$	Date of change from arrivals policy phase 2 to 3
$\tau_3 = 1$ July	Date of final distancing restriction
$T = 2020\text{-}06\text{-}07$	Date of most recent mobility data
$g^*(t) = \int_{t-1}^{t} \text{lognormal}(\tau \mid 1.377, 0.567^2)\, \text{d}\tau$	Baseline generation interval function

Table S3: Parameters used in the timeseries part of the time-varying model of R_{eff}.

Prior distribution	Parameter description
$\sigma_1 \sim \text{N}^+(0, 0.5^2)$	Hierarchical component of amplitude of deviation; import-local R_{eff}
$\sigma_{i,1} \sim \text{N}^+(0, 0.5^2)$	State-level component of amplitude of deviation; import-local R_{eff}
$l_1 \sim \text{lognormal}(3, 1)$	Temporal correlation; import-local R_{eff}
$\sigma_2 \sim \text{N}^+(0, 0.5^2)$	Hierarchical component of amplitude of deviation; local-local R_{eff}
$\sigma_{i,2} \sim \text{N}^+(0, 0.5^2)$	State-level component of amplitude of deviation; local-local R_{eff}
$l_2 \sim \text{lognormal}(3, 1)$	Temporal correlation; local-local R_{eff}
$\alpha_2 \sim \text{lognormal}(3, 1)$	Correlation mixture weights; local-local R_{eff}

Supplement: ensemble forecasts of the daily number of new local cases

Methodological details for each of the forecast models in the ensemble are provided below.

1. SEEIIR Forecast

Model Description

We used a discrete-time stochastic SEEIIR model to characterise infection in each Australian jurisdiction. Let $S(t)$ represent the number of *susceptible* individuals, $E_1(t) + E_2(t)$ represent the number of *exposed* individuals, $I_1(t) + I_2(t)$ represent the number of *infectious* individuals, and $R(t)$ the number of *removed* individuals, at time t. Symptom onset is assumed to coincide with the transition from I_1 to I_2. Note that the two exposed and infectious classes are specified in order to obtain a Gamma distribution (with shape parameter 2) on the duration of time in the exposed and infectious classes, respectively. It is assumed that 10 exposures were introduced into the E_1 compartment at time τ, to be inferred, giving initial conditions:

$$
\begin{aligned}
S(0) &= N - E_1(0) & E_1(0) &= 10 \\
E_2(0) &= 0 & I_1(0) &= 0 \\
I_2(0) &= 0 & R(0) &= 0 \\
\sigma(t) &= \begin{cases} 0 & \text{if } t < \tau \\ \sigma & \text{if } t \geq \tau \end{cases} & \gamma(t) &= \begin{cases} 0 & \text{if } t < \tau \\ \gamma & \text{if } t \geq \tau \end{cases} \\
\beta(t) &= R_{\text{eff}}(t) \cdot \gamma(t)
\end{aligned}
$$

The number of individuals leaving each compartment on each *daily* time-step follows a Binomial distribution, as follows:

$$
\begin{aligned}
S &= 1 - \exp\left(-\beta(t) \cdot \left[I_1(t) + I_2(t)\right]/N\right) & S &\sim Bin(S(t), S) \\
E_1 &= 1 - \exp\left(2 \cdot \sigma(t)\right) & E_1 &\sim Bin(E_1(t), E_1) \\
E_2 &= 1 - \exp\left(2 \cdot \sigma(t)\right) & E_2 &\sim Bin(E_2(t), E_2) \\
I_1 &= 1 - \exp\left(2 \cdot \gamma(t)\right) & I_1 &\sim Bin(I_1(t), I_1) \\
I_2 &= 1 - \exp\left(2 \cdot \gamma(t)\right) & I_2 &\sim Bin(I_2(t), I_2) \\
S(t+1) &= S(t) - S & E_1(t+1) &= E_1(t) + S - E_1 \\
E_2(t+1) &= E_2(t) + E_1 - E_2 & I_1(t+1) &= I_1(t) + E_2 - I_1 \\
I_2(t+1) &= I_2(t) + I_1 - I_2 & R(t+1) &= R(t) + I_2
\end{aligned}
$$

We modelled the relationship between model incidence and the observed daily COVID-19 case counts (y_t) using a Negative Binomial distribution with dispersion parameter k, since the data are non-negative integer counts and are over-dispersed when compared to a Poisson distribution. Let X(t) represent the state of the dynamic process *and* particle filter particles at time t, and x_t represent a realisation, i.e., $x_t = (s_t, e_{1t}, e_{2t}, i_{1t}, i_{2t}, r_t, \sigma_t, \gamma_t, \beta_t)$. The probability of being observed (i.e., of being reported as a notifiable case) is the product of two probabilities: that of entering the I_2 compartment, $p_{\text{inc}}(t)$, and the observation probability p_{obs}. In order to improve the stability of the particle filter for very low (or zero) incidence, we also allowed for the possibility of a very small number of observed cases that are *not* directly a result of the

community-level epidemic dynamics (bg_{obs}). The observation process is thus defined as:

$$\begin{aligned}\mathcal{L}(y_t \mid x_t) &\sim (\mathbb{E}[y_t], k)\\ \mathbb{E}[y_t] &= (1 - p_{\text{inc}}(t)) \cdot bg_{\text{obs}} + p_{\text{inc}}(t) \cdot p_{\text{obs}} \cdot N\\ p_{\text{inc}}(t) &= \frac{I_2(t) + R(t) - I_2(t-1) - R(t-1)}{N}\end{aligned}$$

We used a bootstrap particle filter, as previously described in the context of our Australian seasonal influenza forecasts [10, 11, 12, 13, 14], to generate forecasts at each day.

Parameters and model prior distributions

		Description	Value
(i)	N	The population size	Table S5
	$R_{\text{eff}}(t)$	The time-varying effective reproduction number	See text
	σ	The inverse of the latent period (days^{-1})	See text
	γ	The inverse of the infectious period (days^{-1})	See text
	τ	The time of the initial exposures (days)	$\sim \mathcal{U}(0, 50)$
(ii)	bg_{obs}	The background observation rate	0.05
	p_{obs}	The observation probability	0.8
	k	The dispersion parameter	10
(iii)	N_{px}	The number of particles	2000
	N_{min}	The minimum number of effective particles	$0.25 \cdot N_{px}$

Table S4: Parameter values for (i) the transmission model; (ii) the observation model; and (iii) the bootstrap particle filter.

Jurisdiction	N
Australian Capital Territory	410,199
New South Wales	5,730,000
Queensland	2,560,000
South Australia	1,408,000
Northern Territory	154,280
Tasmania	240,342
Victoria	5,191,000
Western Australia	2,385,000

Table S5: The population sizes used for each forecast.

Model and inference parameters are described in Table S4. Note that the transmission model assumes that the population mixes homogeneously. Since Australia is one of the most urbanised countries in the world, for each jurisdiction we used capital city residential populations (including the entire metropolitan region, as listed in Table S5) in lieu of the residential population of each jurisdiction as a whole.

The prior distributions for $R_{\text{eff}}(t)$, σ, and γ were constructed in a separate analysis, not described here. Parameters σ and γ were sampled from a multivariate log-normal distribution

that was defined to be consistent with a generation interval with mean=4.7 and SD=2.9, and sampled independent $R_{\text{eff}}(t)$ trajectories for each particle.

2. Probabilistic Forecast

We provide a generative model of the dynamics of SARS-CoV-2 in Australia. This allows us to forecast COVID-19 cases by state/territory, and nationally. The model links distancing measures – captured via Google Mobility Indices, and an estimated "Micro-distancing" parameter – to the effective reproduction number of local infectious individuals, allowing us to produce forecasts under scenarios of change in Government-imposed distancing measures.

Inferring Effective Reproduction Numbers and Social Isolation Measures
Using the method from Abbott et al. [3], and case data provided by the National Notifiable Disease Surveillance System (NNDSS), we produce estimates of the effective reproduction number R_{eff}. The model described below relates population mobility measures to this R_{eff} estimate and is then used to project the reproduction number forward in order to generate forecasts of cases.

These estimates of the effective reproduction numbers are assumed to be dependent upon the proportion of observed imported cases out of all observed cases (ρ), the impact of "macro" social isolation measures — captured via Google Mobility Indices ($\boldsymbol{\omega}(t)$) — and "micro-distancing" (M_d).

We link these previous estimates of the effective reproduction number with the distancing measures via the model:

$$\hat{\mu}(t) = \rho(t)R_I + (1 - \rho(t))\, R_L(t), \tag{37}$$

$$R_L(t) = R_{L0} M_d^{1_{\{\text{post-ban}\}}} \times 2 \times \text{logistic}\left(\boldsymbol{\beta}^{\boldsymbol{T}} \boldsymbol{\omega}(t)\right) \tag{38}$$

in which:

- $\rho(t)$ (inferred; State level) is the proportion of imported cases (of all cases) on day t;
- R_I (inferred; national level) is the effective reproduction number of imported cases;
- R_{L0} (inferred; national level) is the effective reproduction number of local symptomatic cases at base levels of mobility;
- M_d (inferred; national level) is a micro-distancing factor, which allows for the effective reproduction number of local cases to be reduced post 16/03/2020 ($1_{\{\text{post-ban}\}}$ is an indicator function that takes value 0 or 1, pre- or post- specified date, respectively);
- $\boldsymbol{\beta}$ (inferred; national level) is a vector of parameters that link Google Mobility Indices to the effective reproduction number of local cases via the logistic function, which ranges between 0 and 1; and,
- $\boldsymbol{\omega}(t)$ (state level) are the 7-day future moving average of Google Mobility Indices on day t.

We assume that (the likelihood)

$$\hat{\mu}(t) \sim \text{Gamma}(k(t), \theta(t)),$$

with $k(t) = \frac{R_{\text{eff}}(t)^2}{\sigma^2(t)}$ and $\theta(t) = \frac{\sigma^2(t)}{R_{\text{eff}}(t)}$, to match the distribution of R_{eff} estimates from earlier work [15].

We perform inference in a Bayesian framework, using Hamiltonian Monte Carlo through the software package `pystan` [16]. Prior distributions for the parameters are:

$$\begin{aligned}
\rho(t) &\sim \text{Beta}\left(1 + I(t), 1 + L(t)\right); \\
\boldsymbol{\beta} &\sim \text{Normal}(0, 1); \\
R_I &\sim \text{Gamma}(1.25, 0.4); \\
R_{L0} &\sim \text{Gamma}(2.4, 1); \text{and}, \\
M_d &\sim \text{Gamma}(0.5, 1),
\end{aligned}$$

where $I(t)$ and $L(t)$ are the number of imported and local cases on day t respectively.

We use case data for every Australian state/territory through the month of March, and generate the posterior predictive distribution of the reproduction number in each jurisdiction over time.

Forecasts of mobility indices

Our forecasts are produced by first forecasting (using a random walk with drift) the Google Mobility Indices. For each Google mobility index, the differences in each successive day were assumed to be normally distributed and used to estimate the mean and variance (for each state/territory). This is done for the 28 days preceding the last Google mobility index entry at the time the forecast is generated. The index is then forecast for the next 50 days by successively adding a sample from the estimated normal distribution each day. Each index is capped at a maximum of 0% and minimum -50% of the baseline to maintain reasonable estimates of the trend.

The forecast Google mobility indices for each state/territory are then used to create a posterior prediction of the local effective reproduction number, R_L using Equation 38. To account for waning in micro-distancing, after 01/06/2020, the effect of M_d is halved when forecasting the posterior prediction for R_L.

Using the posterior distribution of the parameters relating R_{eff} to the Google mobility indices, we generate posterior predictive distributions of R_L over time using Equation 38 for each jurisdiction and the forecast Google mobility indices.

Generative model

We simulate the number of cases using a branching process based on the estimated reproduction number described above. The generative model contains three types of infectious individuals: Imported (I_I); Asymptomatic (I_A), and; Symptomatic (I_S).

Secondary cases

Each case is assumed to generate a number of cases drawn from a Negative Binomial distribution, with parameters k and, $R_I/(R_I + k)$, $\alpha_A R_L/(\alpha_A R_L + k)$, $\alpha_S R_L/(\alpha_S R_L + k)$ for imported, asymptomatic and symptomatic individuals, respectively.

The parameters R_I and R_L (the effective reproduction numbers for import-to-local and local-to-local cases, respectively) are sampled from the posterior distributions described above. The parameter k is fixed at 0.1 in our analysis, according to existing estimates [17]. This value allows for heterogeneity in the transmissibility of individuals — so-called *super spreading* — in that the mean is realised with high variance. The parameter α_S corresponds to the contribution of transmissibility of symptomatic local cases and the parameter α_A corresponds to the contribution of transmissibility of asymptomatic local cases.

The R_{eff} estimate generated via [3] using the NNDSS case data does not readily distinguish between symptomatic and asymptomatic cases, and cases observed in this initial outbreak are

Table S6: Detection probabilities of Symptomatic, Asymptomatic and Imported cases for each jurisdiction.

Jurisdiction	q_S	q_A	q_I
NSW	0.50	0.10	0.95
QLD	0.40	0.05	0.95
SA	0.38	0.05	0.95
TAS	0.30	0.05	0.95
VIC	0.56	0.13	0.95
WA	0.38	0.05	0.95
ACT	0.80	0.20	0.95
NT	0.80	0.20	0.95

all assumed to be symptomatic. The effective reproduction number is the average number of secondary infections caused by an infected individual, and can be characterised as

$$R_{\text{eff}} = \frac{s_{t+1}}{s_t}, \tag{39}$$

where s_t is the number of detected symptomatic cases in generation t.

In order to correctly attribute the contributions of symptomatic and asymptomatic cases to secondary cases, we require

$$s_{t+1} = (S_t \alpha_S R_L + A_t \alpha_A R_L) p_S q_S \tag{40}$$

where S_t is the true number of local symptomatic cases (*i.e.*, consisting of both observed and unobserved cases), A_t is the true number of local asymptomatic cases, p_S is the probability of being symptomatic and q_S is the probability of detecting a local symptomatic case.

Using Equations 39 and 40, and for local cases where $R_{\text{eff}} = R_L$, we have

$$\alpha_S p_S + \alpha_A (1 - p_S) = 1 \tag{41}$$

In this forecast we assume that p_s is 0.2 and the relative infectiousness of asymptomatic cases is 0.5 of symptomatic cases. It follows from equation 41 that $\alpha_S = 1.67$ and $\alpha_A = 0.833$.

The generative model must also consider probabilities of observing infectious cases. Infectious individuals are detected, and hence become a case, with probabilities q_I, q_A and q_S respectively. Table S6 contains the values used in this forecast.

Time distributions

For each infectious individual, we generate the time that they became infected. This time is randomly generated by adding to the infection time of the individual that infected them, one day plus a random time generated from a Gamma distribution (with shape=1 and scale=2). This corresponds to a 'Generation Time' distribution with mean 3 days and variance 3.91. This is based upon estimates of the generation interval distribution from the literature, and sympathetic to our parameterisation of the Incubation Period distribution. The Incubation Period distribution — the delay between infection and symptom onset — is two days plus a randomly sampled time from a Gamma distribution (with shape=1 and scale=2) with mean 4 days and variance 3.91.

Imports

We additionally assume a Poisson number of new imported infectious individuals on day t, where mean parameter λ_t is inferred from data. We use six time periods ($i = 1, \ldots, 6$) corresponding to:

- 01/03/2020 to 06/03/2020;
- 07/03/2020 to 13/03/2020;
- 14/03/2020 to 18/03/2020;
- 19/03/2020 to 23/03/2020;
- 24/03/2020 to 14/04/2020; and,
- 15/04/2020 onwards.

Cases were classified as imported or locally-acquired according to their reported place of acquisition. If place of acquisition is unknown or missing, the cases were assumed to be locally acquired. In the event that symptom onset date is missing, the date is inferred as follows: notification date - 5 if notification date is recorded, otherwise, notification receive date - 6.

To assign the imported cases to the period in which they are likely to have arrived (as infectious), we have subtracted 4 days from their symptom onset date. Within each state/territory ($j = 1, \ldots, 8$) and in each period, i, we assume that a Poisson number of imports are subsequently detected, $N_{i,j}$. That is, $N_{i,j} \sim \text{Poisson}(\lambda_{i,j})$, independently on each day.

Assuming *a priori* $\lambda_{i,j} \sim \text{Gamma}(\alpha, \beta)$, we have *a posteriori* that $\lambda_{i,j} \sim \text{Gamma}(a_{i,j}, b_i)$ where

$$a_{i,j} = \begin{cases} \alpha + n_{i,j} & \text{if } i \neq 4, \\ \alpha + 1.3n_{i,j}, & \text{if } i = 4 \end{cases}$$
$$b_i = \beta + m_i,$$

in which $n_{i,j}$ is the total number of detected imported cases in period i in state/territory j, and m_i is the number of days in the period i ($m = (m_1, m_2, m_3, m_4, m_5, m_6) = (6, 8, 4, 5, 22, 152)$). The number of imported infectious individuals in period i in state/territory j, $D_{i,j}$, that are to be subsequently detected are simulated each day from its *posterior predictive distribution*,

$$D_{i,j} \sim \text{NegBin}(a_{i,j}, 1/(b_i + 1)).$$

We specified $\alpha = 1$ and $\beta = 1/5$ for the prior distribution, though this choice has little impact on the posterior distribution. Having generated $d_{i,j}$ for each day in period i in state/territory j, we sum the total number of such cases, $s_{i,j}$. Subsequently, we simulate the total number of undetected imported cases,

$$U_{i,j} \sim \text{NegBin}(s_{i,j}, q_I),$$

where q_I is the detection probability of imported cases. The undetected imported cases are allocated to the days in the period i with equal probability.

This process is simulated first, before seeding with any local cases and simulating forward.

Model Initialisation

Initialisation is based upon the *very early* stages of the outbreak. This is based on the assumption that the observed cases make up a large proportion of initial infections. Considering these as an initial generation is likely reasonable. Specifically:

- Given n_S symptomatic local cases, and n_I imported cases on 01/03/2020, we generate:

  - Undetected symptomatic individuals, $U_S \sim \text{NegBin}(n_S, q_S)$,
  - Undetected imports $U_I \sim \text{NegBin}(n_I, q_I)$; and
  - Asymptomatic individuals, $I_A \sim \text{NegBin}(I_S, p_S)$.

- Assign an infection time to the U_S, U_I and I_A individuals from the Generation Time distribution.

- For any infection time which is after the period being considered, sample those detected with probabilities q_S, q_I and q_A, respectively. For detected and symptomatic cases, sample the time to symptom onset from the Incubation Period distribution.

- For New South Wales and Victoria, q_S, q_I and q_A were assumed to be half that of the other states/territories prior to 15/03/2020, on the basis that these jurisdictions experienced a higher volume of cases in this period.

Model Re-initialisation
Events that are difficult to forecast precisely will occur. These are typically large cluster outbreaks; examples include those in Tasmania and most recently Victoria.

When such outbreaks occur, we add to our model state additional cases determined by performing the initialisation step on the day the threshold is exceeded. These events are detected via a threshold on the cumulative (over a moving 3-day period) cases — i.e., when the moving average exceeds the forecasted cases by a factor of 10. The additional n cases are distributed across the 3-day period by adding $n/6$, $n/3$ and $n/2$ to each corresponding day respectively. Simulations are only permitted to re-initialise a maximum of 10 times. If this is exceeded, the simulation is excluded from the forecast.

Code Availability
The code used to generate the simulated cases can be accessed at the repository `https://github.com/tdennisliu/covid19-forecasting-aus`.

3. Time Series Forecast

We estimated a simple autoregressive model using available case data from many countries, obtained from the Johns Hopkins COVID19 repository. For each state, the model uses data from the previous 11 days to estimate the possible trajectory of cases over the next few weeks.

Model Description
We fit a global autoregressive model to all available data from the Johns Hopkins COVID19 repository.

Some data quality issues were detected and the resulting data cleaned or omitted. In particular:

- data by region in the UK, Spain and Italy were added.

- series with fewer than 500 cumulative cases were removed;

- series with fewer than 15 days of data were removed;

- series with anomalous data were removed (*e.g.*, negative case numbers, or very large step changes).

Let $n_{t,i}$ = the number of daily cases on day t in country (or region) i, and let $y_{t,i} = \log(n_{t,i} + 0.5)$. We fit an autoregressive model of order p:

$$y_{t,i} = \phi_1 y_{t-1,i} + \cdots + \phi_p y_{t-p,i} + \varepsilon_{t,i},$$

where $\varepsilon_{t,i}$ are independent $\mathrm{N}(0, \sigma_i^2)$ errors. The model is estimated using ordinary least squares estimation, with no stationarity constraints. The parameters are scale free other than the error variance σ_i^2. Consequently the model is estimated by first scaling all data to have the same mean and variance, to avoid any one country dominating in the estimation. Then the model is applied to the raw data from each country or region when forecasting.

The value of $p = 11$ is chosen to minimize the average 7-day-ahead mean absolute error on recent Australian data. We can afford to have a large value of p due to the large data set used to estimate the model.

It is not intended to be a model of the disease development, and contains no terms that describe public health measures or related policies. However, the model is highly adaptive to different stages of the pandemic including rapid increases, periods of containment, and periods where there are few cases. Time series models of this kind tend to produce relatively accurate short-term forecasts, but are probably less accurate than epidemiological models in the long-term.

The model code is available at `https://github.com/pmontman/covid19forec`.

References

[1] Laura F. White and Marcello Pagano. A likelihood-based method for real-time estimation of the serial interval and reproductive number of an epidemic. *Stat Med*, 27(16):2999–3016, 2008.

[2] Robin Thompson, Jake Stockwin, Rolina D. van Gaalen, Jonathan Polonsky, Zhian Kamvar, Alex Demarsh, Elisabeth Dahlqwist, Siyang Li, Eve Miguel, Thibaut Jombart, Justin Lessler, Simone Cauchemez, and Anne Cori. Improved inference of time-varying reproduction numbers during infectious disease outbreaks. *Epidemics*, 29:100356, 2019.

[3] Sam Abbott, Joel Hellewell, James Munday, Robin Thompson, and Sebastian Funk. *EpiNow: Estimate realtime case counts and time-varying epidemiological parameters*, 2020. R package version 0.1.0.

[4] David A. Rolls, Nicholas L. Geard, Deborah J. Warr, Paula M. Nathan, Garry L. Robins, Philippa E. Pattison, James M. McCaw, and Jodie McVernon. Social encounter profiles of greater Melbourne residents, by location – a telephone survey. *BMC Infectious Diseases*, 15(1):494, December 2015.

[5] Kiesha Prem, Alex R. Cook, and Mark Jit. Projecting social contact matrices in 152 countries using contact surveys and demographic data. *PLOS Computational Biology*, 13(9):1–21, 09 2017.

[6] Hiroshi Nishiura, Natalie M Linton, and Andrei R Akhmetzhanov. Serial interval of novel coronavirus (COVID-19) infections. *Int J Infect Dis*, 93:284–6, 2020.

[7] Seth Flaxman, Swapnil Mishra, Axel Gandy, Juliette T Unwin, Helen Coupland, Thomas A Mellan, Harrison Zhu, Tresnia Berah, Jeffrey W Eaton, Pablo NP Guzman, Nora Schmit, Lucia Cilloni, Kylie EC Ainslie, Marc Baguelin, Isobel Blake, Adhiratha Boonyasiri, Olivia Boyd, Lorenzo Cattarino, Constanze Ciavarella, Laura Cooper, Zulma Cucunubá, Gina Cuomo-Dannenburg, Amy Dighe, Bimandra Djaafara, Ilaria Dorigatti, Sabine van Elsland, Rich FitzJohn, Han Fu, Katy Gaythorpe, Lily Geidelberg, Nicholas Grassly, Will Green, Timothy Hallett, Arran Hamlet, Wes Hinsley, Ben Jeffrey, David Jorgensen, Edward Knock, Daniel Laydon, Gemma Nedjati-Gilani, Pierre Nouvellet, Kris Parag, Igor Siveroni, Hayley Thompson, Robert Verity, Erik Volz, Caroline Walters, Haowei Wang, Yuanrong Wang, Oliver Watson, Xiaoyue Xi Peter Winskill, Charles Whittaker, Patrick GT Walker, Azra Ghani, Christl A Donnelly, Steven Riley, Lucy C Okell, Michaela AC Vollmer, Neil M. Ferguson, and Samir Bhatt. Report 13: Estimating the number of infections and the impact of non-pharmaceutical interventions on COVID-19 in 11 European countries. 2020.

[8] Nick Golding. greta: simple and scalable statistical modelling in r. *Journal of Open Source Software*, 4(40):1601, 2019.

[9] Nick Golding. *greta.gp: Gaussian Process Modelling in greta*, 2020. R package version 0.1.5.9001.

[10] Robert Moss, Alex Zarebski, Peter Dawson, and James M. McCaw. Forecasting influenza outbreak dynamics in Melbourne from Internet search query surveillance data. *Influenza and Other Respiratory Viruses*, 10(4):314–323, July 2016.

[11] Robert Moss, Alex Zarebski, Peter Dawson, and James M. McCaw. Retrospective forecasting of the 2010–14 Melbourne influenza seasons using multiple surveillance systems. *Epidemiology and Infection*, 145(1):156–169, January 2017.

[12] Robert Moss, James E. Fielding, Lucinda J. Franklin, Nicola Stephens, Jodie McVernon, Peter Dawson, and James M. McCaw. Epidemic forecasts as a tool for public health: interpretation and (re)calibration. *Australian and New Zealand Journal of Public Health*, 42(1):69–76, February 2018.

[13] Robert Moss, Alexander E. Zarebski, Sandra J. Carlson, and James M. McCaw. Accounting for healthcare-seeking behaviours and testing practices in real-time influenza forecasts. *Tropical Medicine and Infectious Disease*, 4:12, January 2019.

[14] Robert Moss, Alexander E. Zarebski, Peter Dawson, Lucinda J. Franklin, Frances A. Birrell, and James M. McCaw. Anatomy of a seasonal influenza epidemic forecast. *Communicable Diseases Intelligence*, 43:1–14, March 2019.

[15] David J. Price, Freya M. Shearer, Michael T. Meehan, Emma McBryde, Robert Moss, Nick Golding, Eamon J. Conway, Peter Dawson, Deborah Cromer, James Wood, Sam Abbott, Jodie McVernon, and James M. McCaw. Early analysis of the australian covid-19 epidemic. *medRxiv*, 2020.

[16] Stan Development Team. Stan Modeling Language: User's Guide and Reference Manual. *Version 2.17.0*, 2017.

[17] Akira Endo, Centre for the Mathematical Modelling of Infectious Diseases COVID-19 Working Group, Sam Abbott, Adam J. Kucharski, and Sebastian Funk. Estimating the overdispersion in COVID-19 transmission using outbreak sizes outside China. *Wellcome Open Research*, 5:67, 2020.

Supplementary figures

Figure S2: Time series of new daily confirmed cases of COVID-19 in Australia (purple = overseas acquired, blue = locally acquired, green = unknown) from 14 February to 5 July 2020. Plotted by recorded or inferred date of symptom onset.

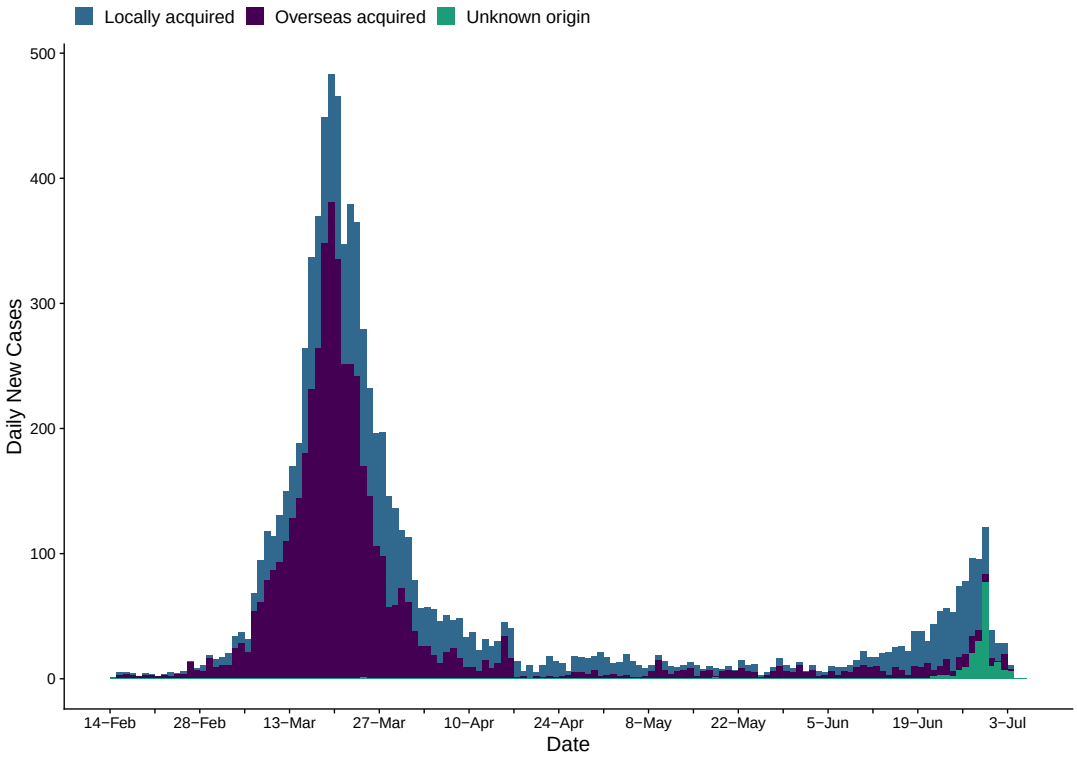

Figure S3: Time series of new daily confirmed cases of COVID-19 in each Australian state/territory (purple = overseas acquired, blue = locally acquired, green = unknown) from 14 February to 5 July 2020. Plotted by recorded or inferred date of symptom onset. Note that y-axis scales differ between states/territories.

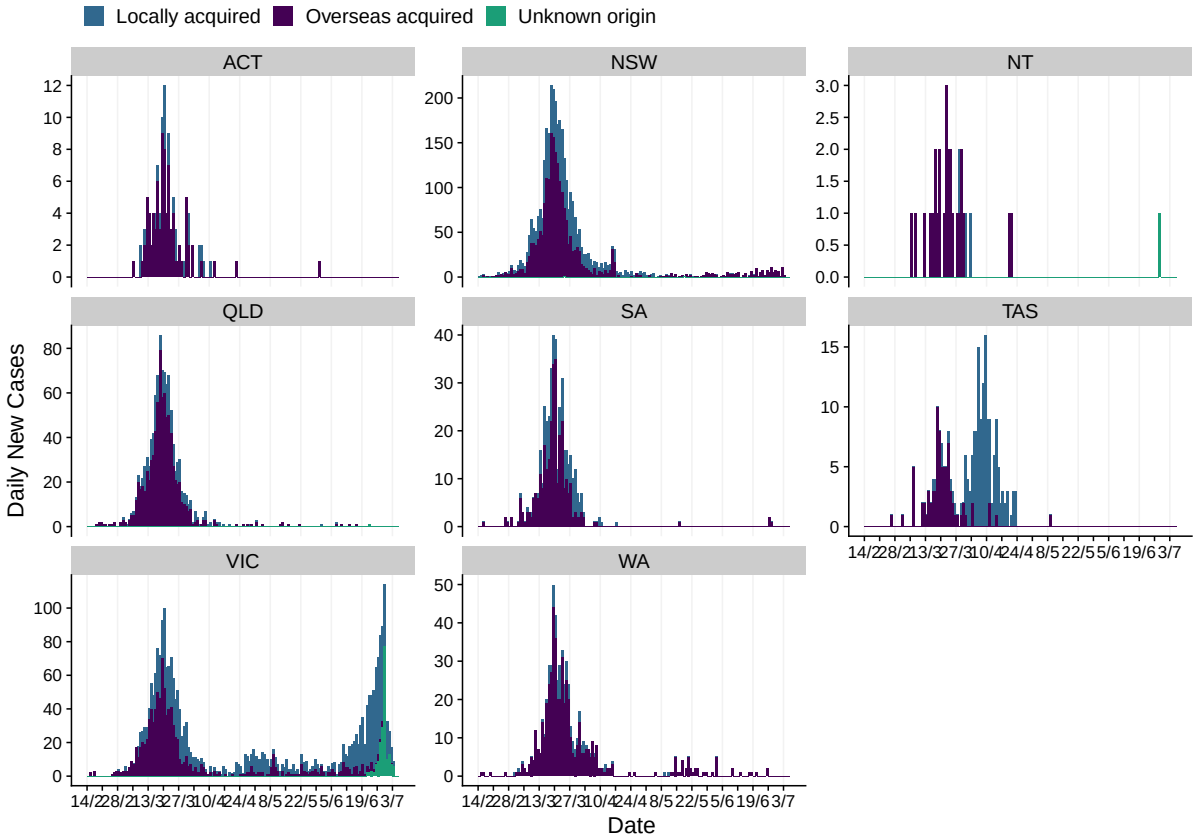

Figure S4: Estimated change in the distribution of times from symptom onset to detection for locally-acquired cases (black line = median time to detection; yellow ribbon = 90% quantile of distribution; black dots = time-to-detection of each case). Future changes in testing strategies, particularly the increasing use of serological assays for case ascertainment, may require changes to the model used to capture this trend and account for it in estimates of transmission potential.

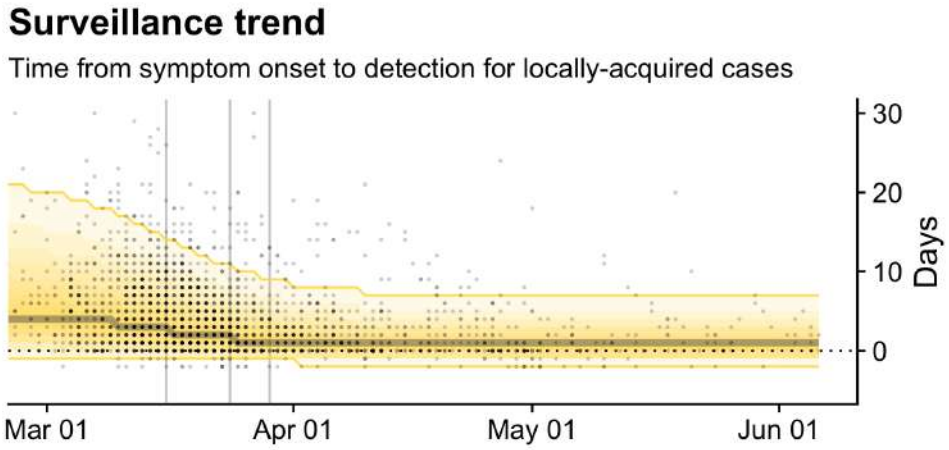

Figure S5: Estimate of average state-level trend in local transmission potential, if we assume that only 'macro-distancing' behaviour had changed and not 'micro-distancing' behaviour or time-to-detection, for each state/territory (light blue ribbon = 90% credible interval; dark blue ribbon = 50% credible interval). Estimates are made up to 1 July, based on cases with inferred infection dates up to and including 1 July. Solid grey vertical lines indicate key dates of implementation of various physical distancing policies. Black dotted line indicates the target value of 1 for the effective reproduction number required for control.

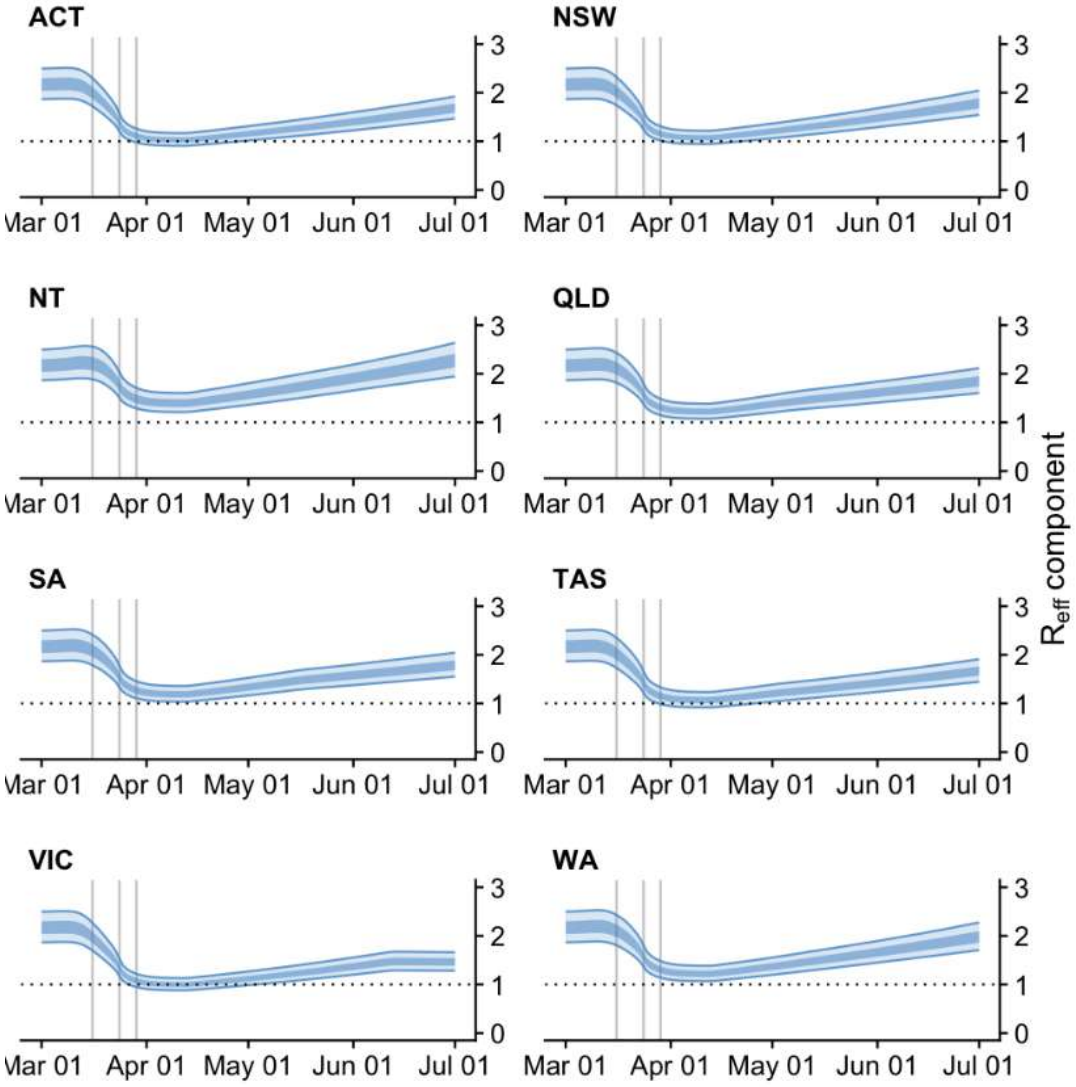

Figure S6: Estimate of average state-level trend in local transmission potential, if we assume that only 'micro-distancing' behaviour had changed and not 'macro-distancing' behaviour or time-to-detection, for each state/territory (light purple ribbon = 90% credible interval; dark purple ribbon = 50% credible interval). Estimates are made up to 1 July, based on cases with inferred infection dates up to and including 1 July. Solid grey vertical lines indicate key dates of implementation of various physical distancing policies. Black dotted line indicates the target value of 1 for the effective reproduction number required for control.

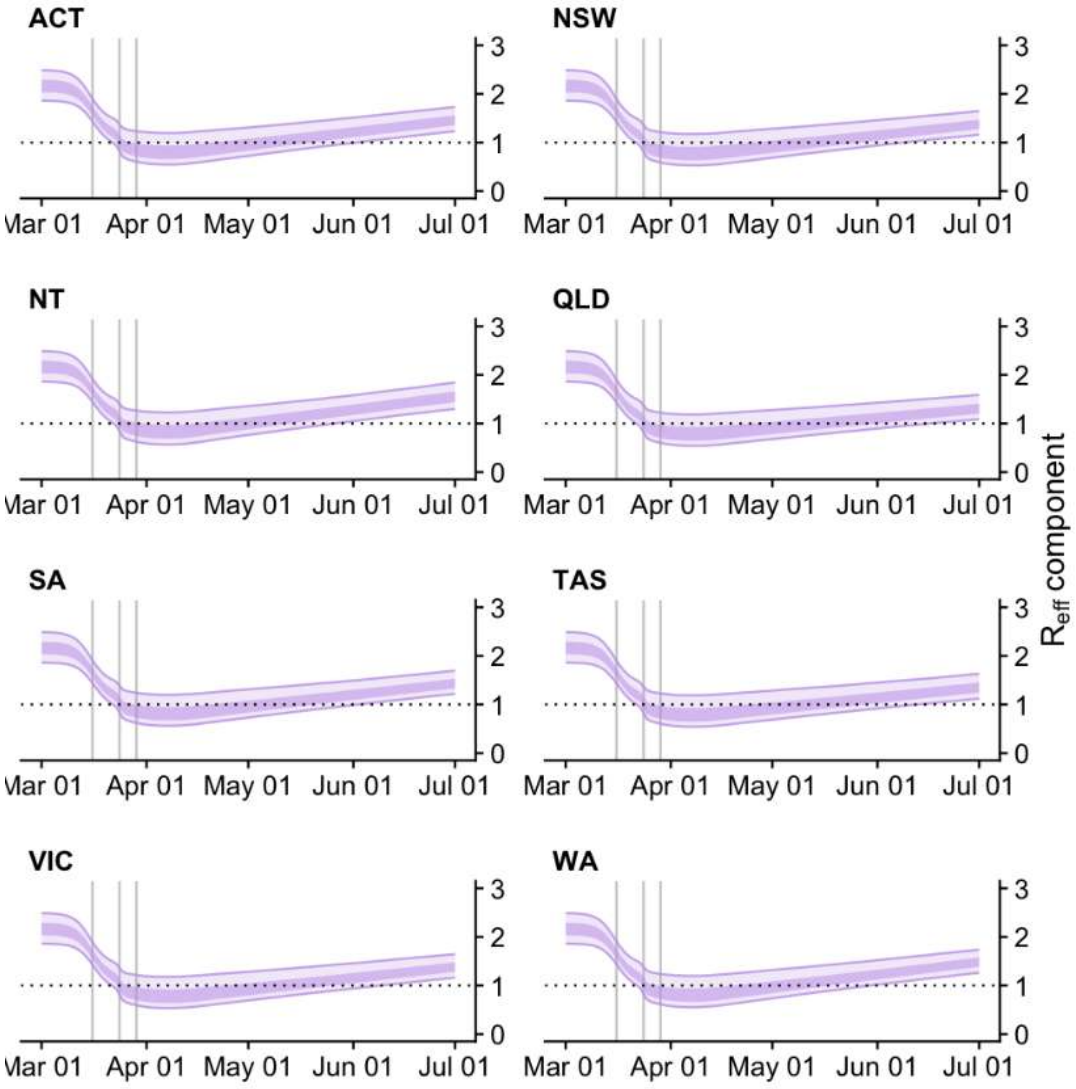

Figure S7: Percentage change compared to a pre-COVID-19 baseline of a number of key mobility data streams in the Australian Capital Territory. Solid vertical lines give the dates of three physical distancing measures: restriction of gatherings to 500 people or fewer; closure of bars, restaurants, and cafes; restriction of gatherings to 2 people or fewer. The dashed vertical line marks the most recent date for which some mobility data are available. Purple dots in each panel are data stream values (percentage change on baseline). Solid lines and grey shaded regions are the posterior mean and 95% credible interval estimated by our model of the latent behavioural factors driving each data stream.

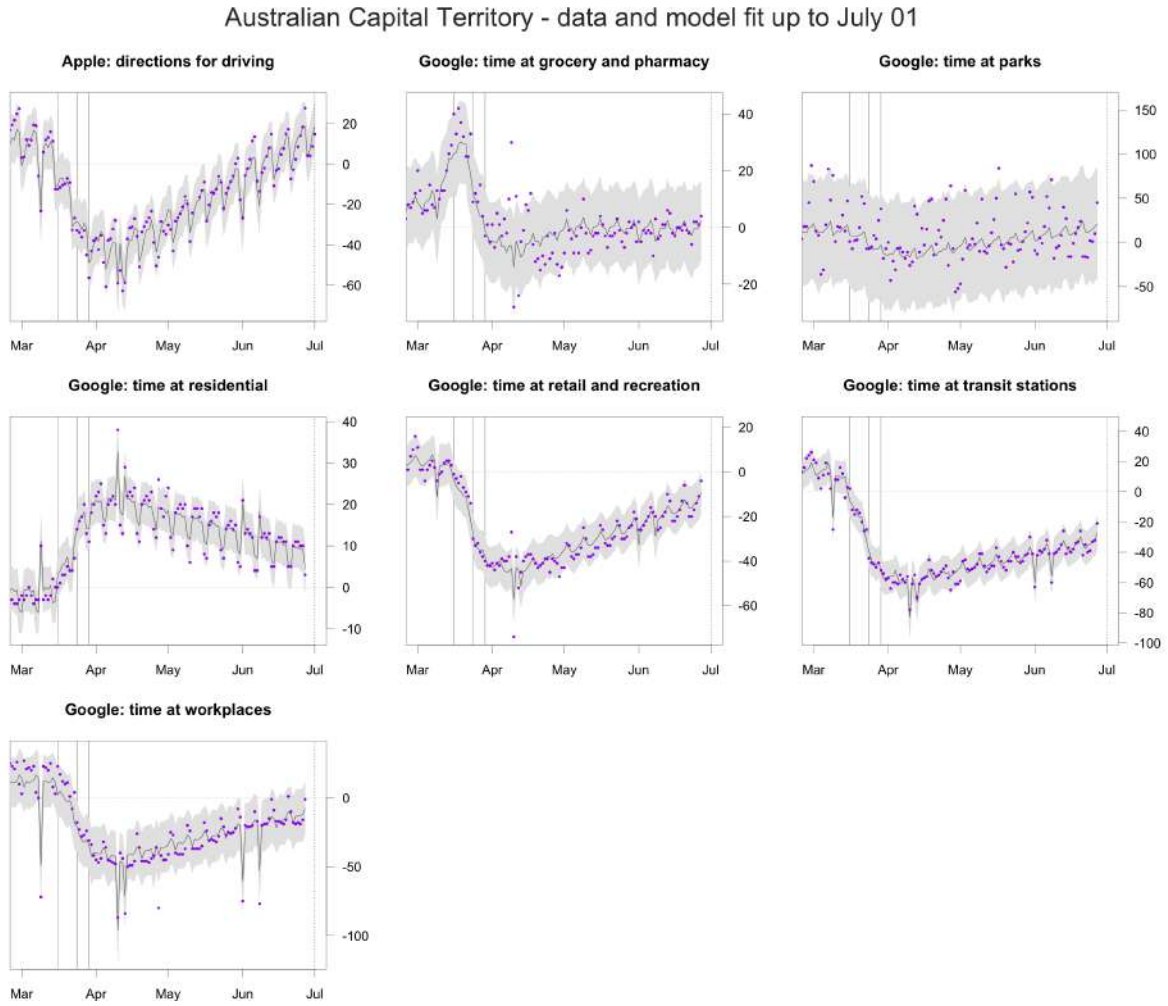

Figure S8: Percentage change compared to a pre-COVID-19 baseline of a number of key mobility data streams in New South Wales. Solid vertical lines give the dates of three physical distancing measures: restriction of gatherings to 500 people or fewer; closure of bars, restaurants, and cafes; restriction of gatherings to 2 people or fewer. The dashed vertical line marks the most recent date for which some mobility data are available. Purple dots in each panel are data stream values (percentage change on baseline). Solid lines and grey shaded regions are the posterior mean and 95% credible interval estimated by our model of the latent behavioural factors driving each data stream.

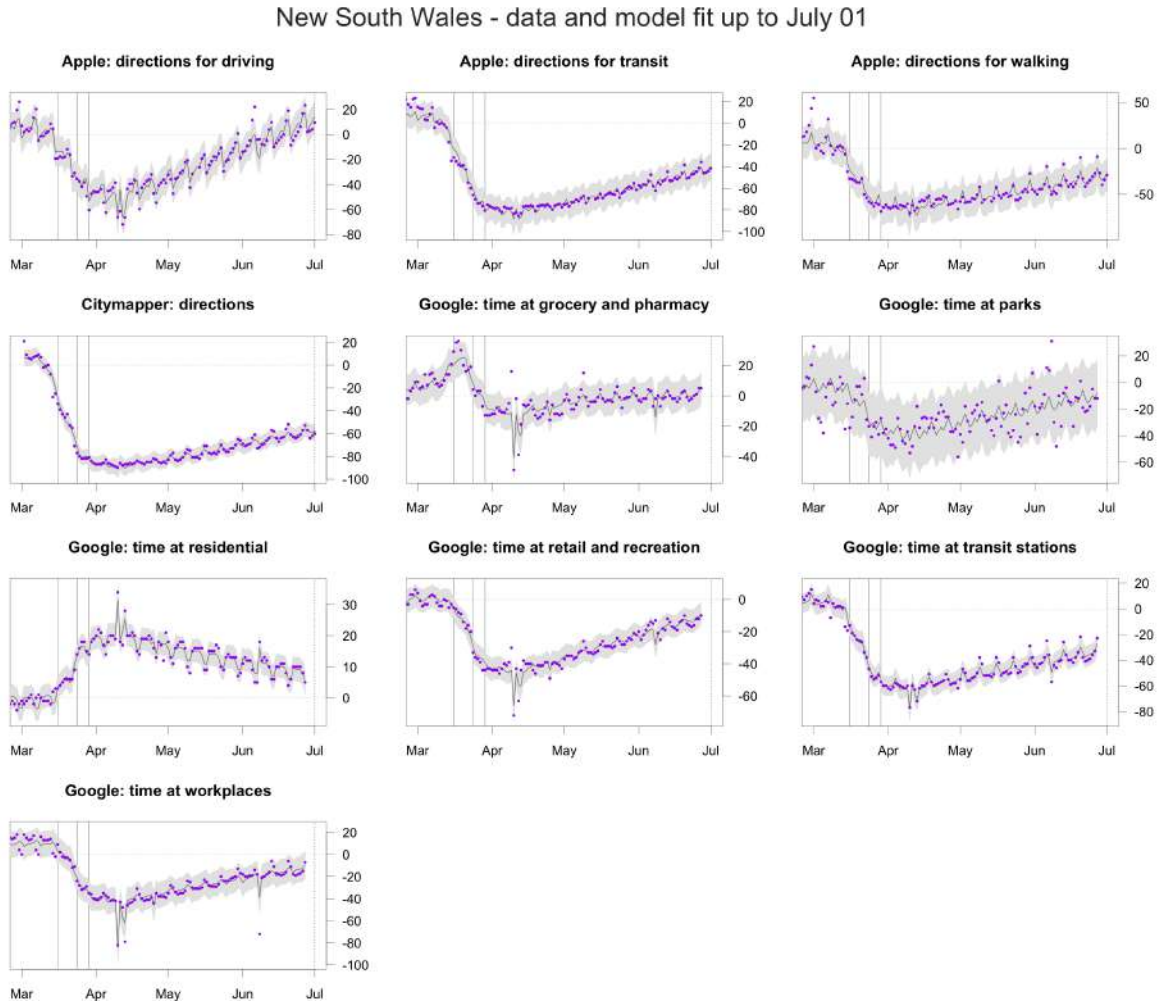

Figure S9: Percentage change compared to a pre-COVID-19 baseline of a number of key mobility data streams in Northern Territory. Solid vertical lines give the dates of three physical distancing measures: restriction of gatherings to 500 people or fewer; closure of bars, restaurants, and cafes; restriction of gatherings to 2 people or fewer. The dashed vertical line marks the most recent date for which some mobility data are available. Purple dots in each panel are data stream values (percentage change on baseline). Solid lines and grey shaded regions are the posterior mean and 95% credible interval estimated by our model of the latent behavioural factors driving each data stream.

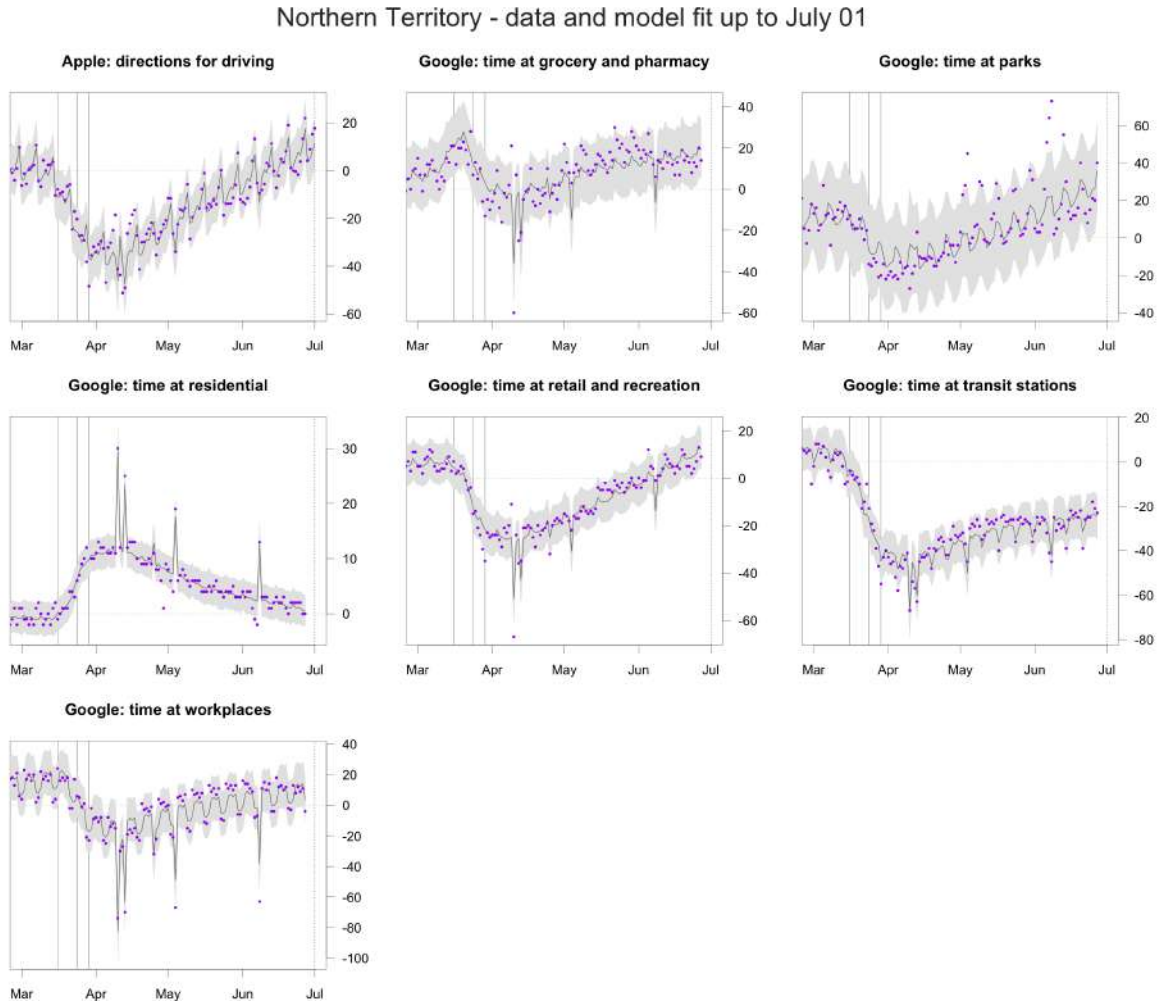

Figure S10: Percentage change compared to a pre-COVID-19 baseline of a number of key mobility data streams in Queensland. Solid vertical lines give the dates of three physical distancing measures: restriction of gatherings to 500 people or fewer; closure of bars, restaurants, and cafes; restriction of gatherings to 2 people or fewer. The dashed vertical line marks the most recent date for which some mobility data are available. Purple dots in each panel are data stream values (percentage change on baseline). Solid lines and grey shaded regions are the posterior mean and 95% credible interval estimated by our model of the latent behavioural factors driving each data stream.

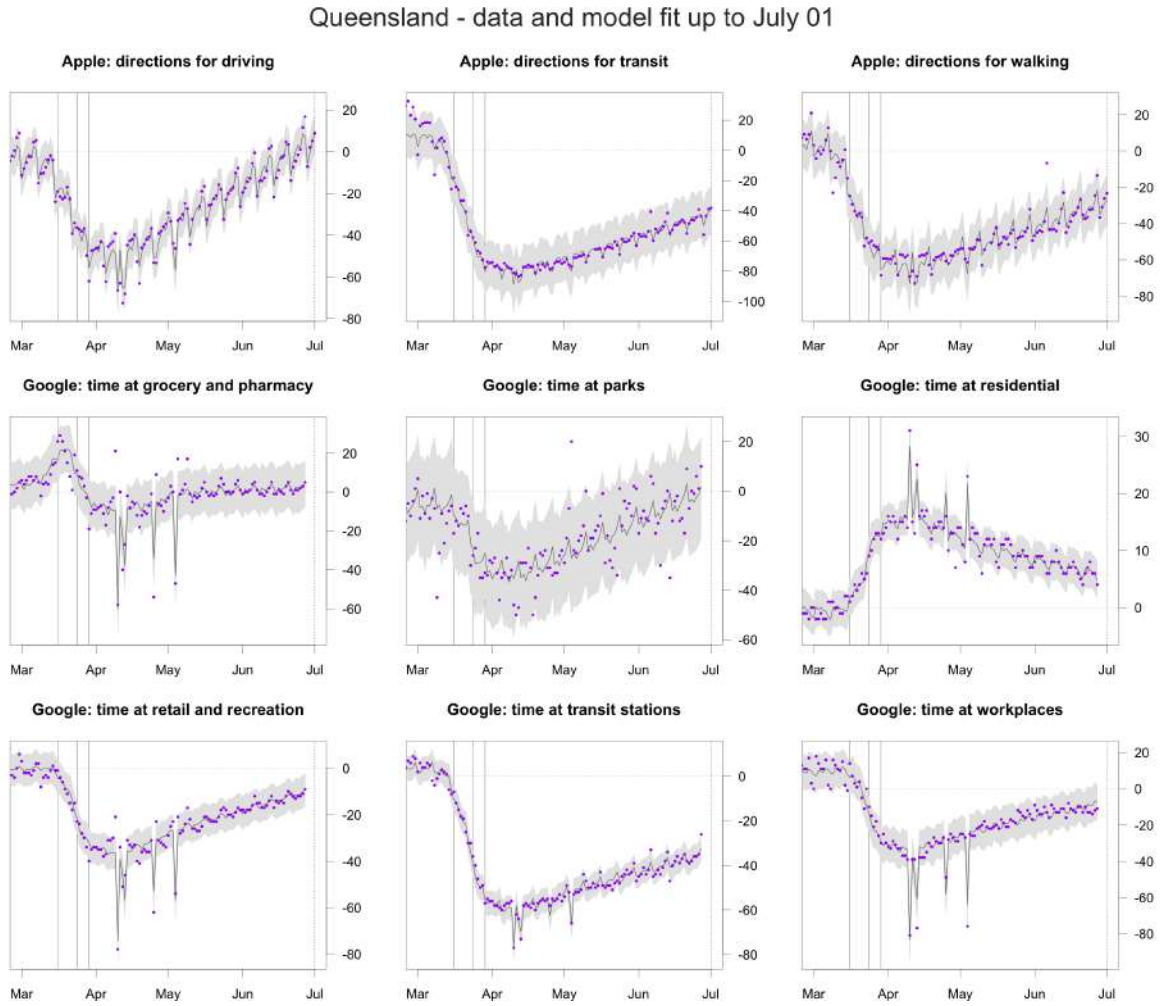

Figure S11: Percentage change compared to a pre-COVID-19 baseline of a number of key mobility data streams in South Australia. Solid vertical lines give the dates of three physical distancing measures: restriction of gatherings to 500 people or fewer; closure of bars, restaurants, and cafes; restriction of gatherings to 2 people or fewer. The dashed vertical line marks the most recent date for which some mobility data are available. Purple dots in each panel are data stream values (percentage change on baseline). Solid lines and grey shaded regions are the posterior mean and 95% credible interval estimated by our model of the latent behavioural factors driving each data stream.

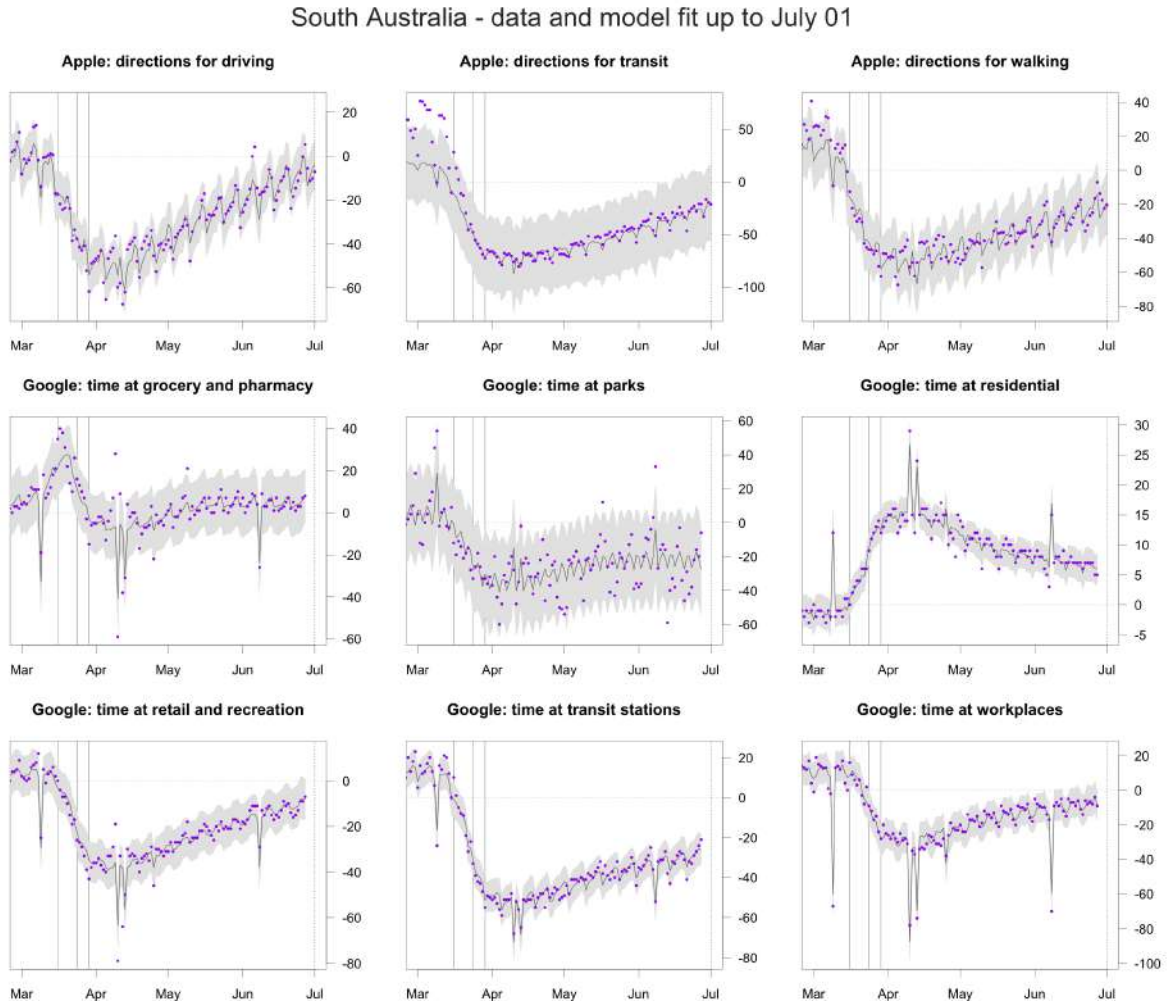

Figure S12: Percentage change compared to a pre-COVID-19 baseline of a number of key mobility data streams in Tasmania. Solid vertical lines give the dates of three physical distancing measures: restriction of gatherings to 500 people or fewer; closure of bars, restaurants, and cafes; restriction of gatherings to 2 people or fewer. The dashed vertical line marks the most recent date for which some mobility data are available. Purple dots in each panel are data stream values (percentage change on baseline). Solid lines and grey shaded regions are the posterior mean and 95% credible interval estimated by our model of the latent behavioural factors driving each data stream.

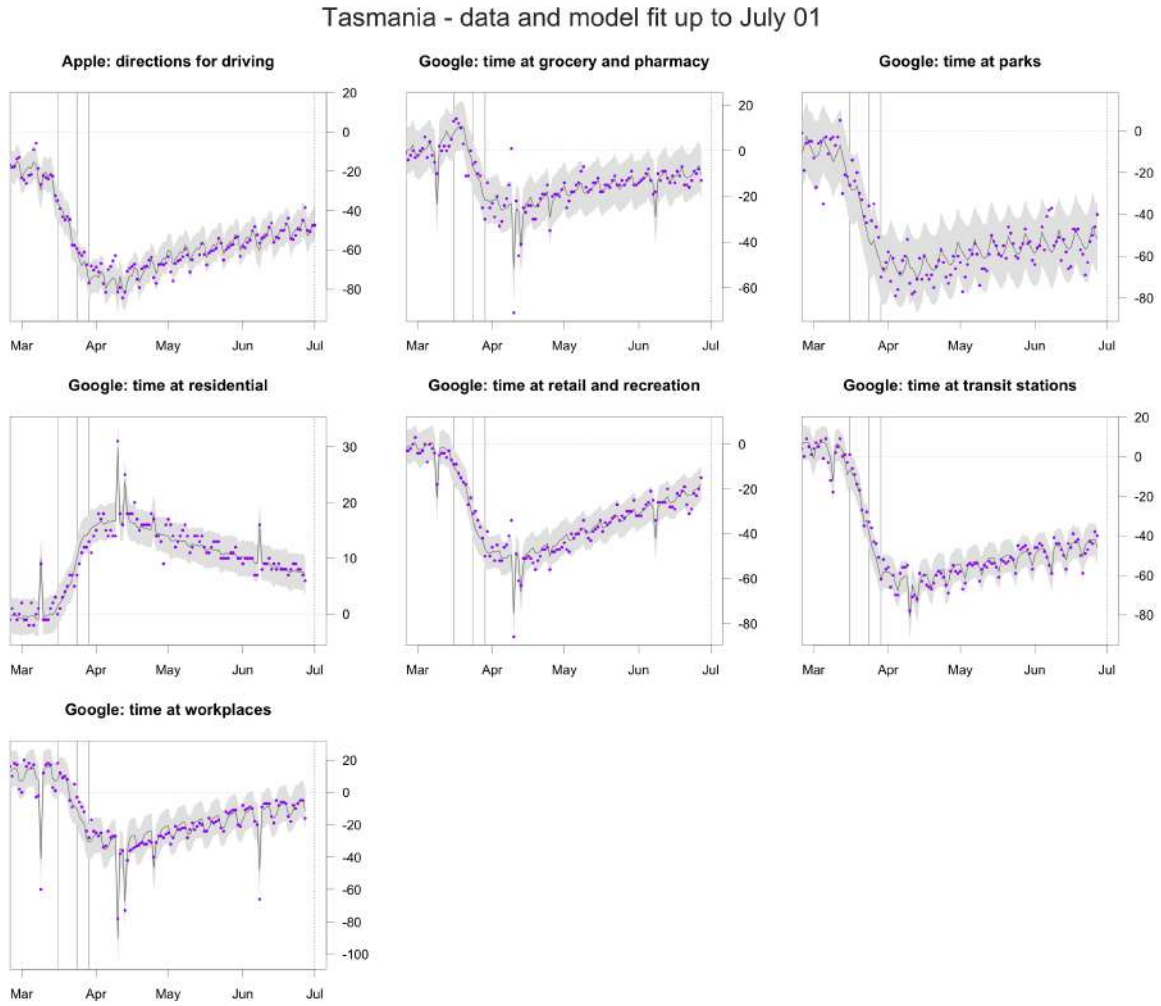

Figure S13: Percentage change compared to a pre-COVID-19 baseline of a number of key mobility data streams in Victoria. Solid vertical lines give the dates of three physical distancing measures: restriction of gatherings to 500 people or fewer; closure of bars, restaurants, and cafes; restriction of gatherings to 2 people or fewer. The dashed vertical line marks the most recent date for which some mobility data are available. Purple dots in each panel are data stream values (percentage change on baseline). Solid lines and grey shaded regions are the posterior mean and 95% credible interval estimated by our model of the latent behavioural factors driving each data stream.

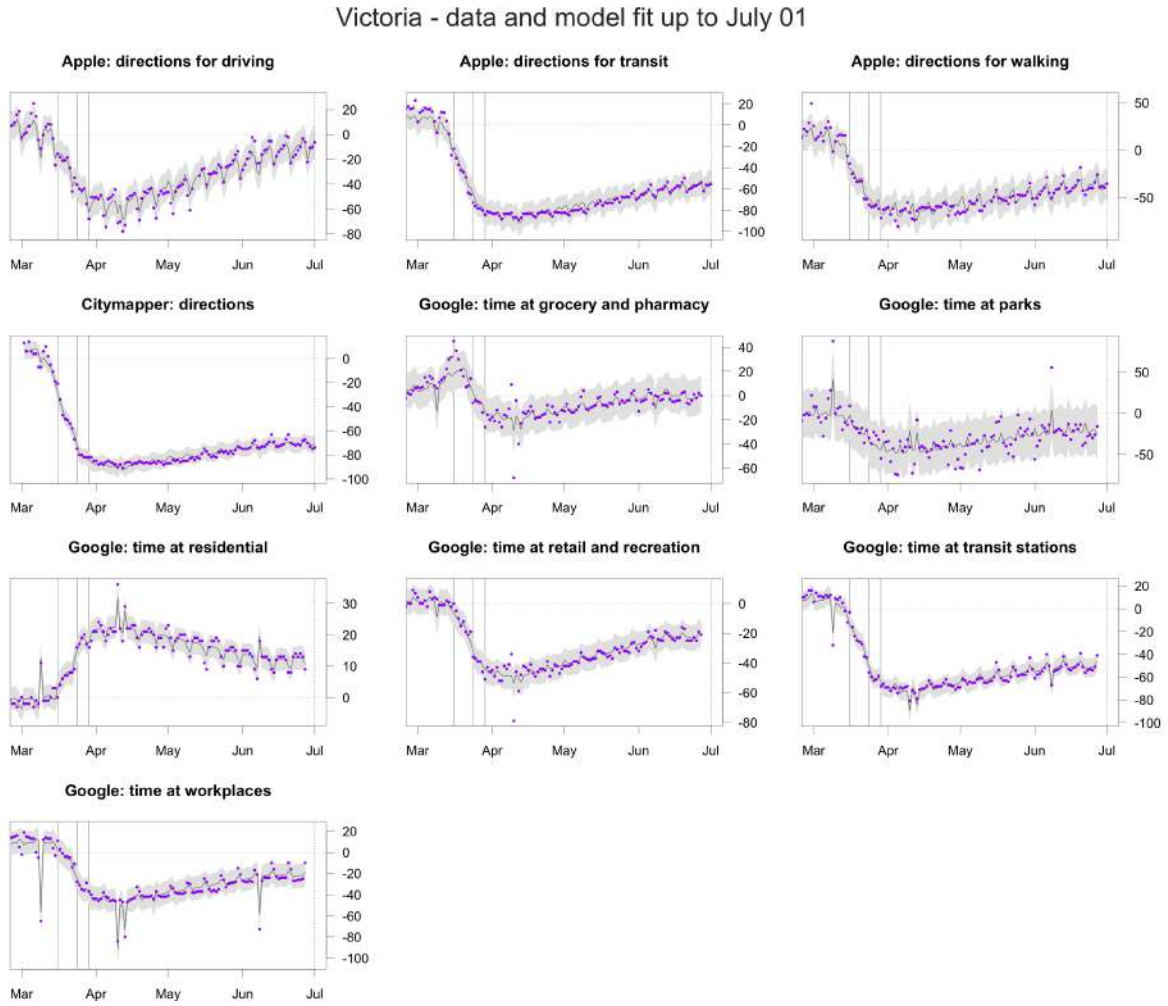
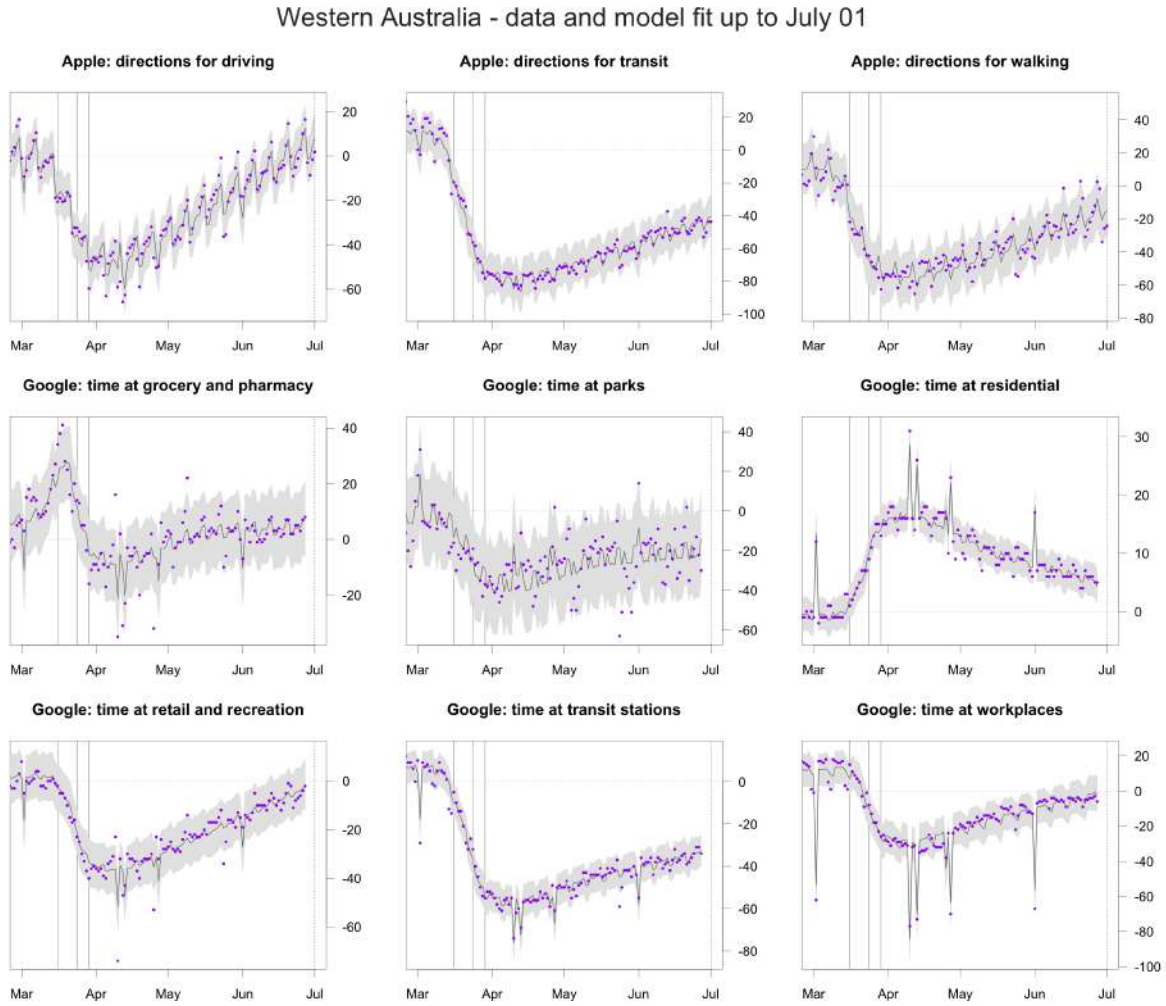
Figure S14: Percentage change compared to a pre-COVID-19 baseline of a number of key mobility data streams in Western Australia. Solid vertical lines give the dates of three physical distancing measures: restriction of gatherings to 500 people or fewer; closure of bars, restaurants, and cafes; restriction of gatherings to 2 people or fewer. The dashed vertical line marks the most recent date for which some mobility data are available. Purple dots in each panel are data stream values (percentage change on baseline). Solid lines and grey shaded regions are the posterior mean and 95% credible interval estimated by our model of the latent behavioural factors driving each data stream.